AN OVERVIEW OF KEY TECHNOLOGY THRUSTS AT
BELL HELICOPTER TEXTRON

Jim Harse, Jing G. Yen, Rod Taylor

Bell Helicopter Textron Inc.
Fort Worth, Texas

This paper will provide insight into several key technologies at Bell. Specific topics include the results of on-going Independent Research and Development (IR&D) in advanced rotors, methodology development, and new configurations. Each subject area highlights some of the research activity now in progress, its supporting technology development, and the results to date.

The discussion on advanced rotors, in Part I, highlights developments on the composite, bearingless rotor, including the development and testing of full-scale flight hardware as well as some of the design support analyses and verification testing.

The discussion on methodology development, in Part II, concentrates on analytical development in aeromechanics, including correlation studies and design application. Specific emphasis is given to aerodynamic, dynamic, and handling qualities methodologies as they relate to advanced design requirements.

The final topic, new configurations, in Part III, presents the results of some advanced configuration studies, including a report on hardware development in progress.

PART I. ADVANCED ROTORS

The continuing IR&D efforts at Bell cover the entire spectrum of technologies applicable to rotary wing aircraft. From survivability to flight simulation, from advanced material applications to tailored airfoils, achievements in IR&D have made it possible to incorporate enhanced safety, performance, and mission capabilities into future designs, along with lower cost of ownership. This has put Bell in a good position to meet the challenges of the LHX and V-22 programs and remain competitive in the helicopter marketplace. Many contracted R&D programs have been initiated to further explore and refine technologies that have come from Bell IR&D programs.

Since the late 1970's, Bell has concentrated on the use of composite materials in the development of advanced rotor hubs and blades. The evolution of rotor blades from metal to composite materials was straightforward and preceded the development of composite hubs. Composite materials not only made rotor blades corrosion resistant, but the unidirectional properties of these composites resulted in fail-safe structures with unlimited life.

The use of composite materials in rotor blades also provided greater opportunities for performance and vibration optimization through aerodynamic and dynamic tailoring. Bell's contributions to the development of composite rotor blades include the following:

(1) First FAA certification in 1978

(2) Three designs currently in production (all IR&D)

(3) Four prototype designs currently undergoing extensive flight testing (3 IR&D)

(4) Two designs under development and now in the fabrication phase (1 IR&D)

ROTOR HUBS

The application of composite materials to hubs was a much more challenging task because of the design requirements for functionality as well as structural design soundness. The thrust of Bell's efforts was to replace the flap, lag, pitch-change, and blade retention mechanisms with composite structures. The key was to fully exploit the anisotropic properties of composite materials in unique designs, not merely replace the metallic structural hub components that have isotropic loading and support the usual bearings and hinges of conventional hub designs.

The first step was to develop a single structure made of fiberglass/epoxy that could carry all of the flight loads and support the blade retention/pitch change bearings. This structure is referred to as the "yoke" at Bell. In this concept, the yoke also forms a flapping flexure that eliminates the flapping degree-of-freedom from the pitch change bearings, thus making the bearings, bearing support structure of the yoke, and the lead-lag damping mechanism more compact. The resulting hub design is fail-safe because of the composite materials out of which it is made, and maintenance free because of the elastomeric materials in the pitch change bearings and lead-lag dampers.

A composite yoke designed to replace the titanium yoke on the Bell Model 412 rotor hub is now undergoing qualification testing (fig. 1-1). It will be the first hub component to receive on-condition FAA certification. The rotor hubs for the Bell Model OH-58D Army Helicopter Improvement Program (AHIP), which is in production, and the Bell Canada Model 400 also have composite yokes (fig. 1-2). For rotors with pitch change bearings, these designs are structurally efficient because the primary loads are carried by the unidirectional fibers, as in the composite blade designs.

BEARINGLESS HUBS

The next step in rotor hub development at Bell was to eliminate the blade retention/pitch change bearings. The simplicity and weight savings of such a design would be significant because the bulky and heavy bearing housings would be gone and the bearing support structure (with its isotropic loading) would be replaced with an alternate yoke geometry loaded in a more efficient manner. To evaluate the benefits and assess the risks of a bearingless main rotor, Bell initiated the Model 680 program.

After a series of model tests, design layout studies, and dynamic analyses, Bell designed the rotor system shown in figure 1-3. It consists of a one-piece yoke with four arms extending radially from the center area to the blade roots. The shear-restraint pivots are mounted at the inboard end of the yoke and damper sets connect the shear restraints to pitch change cuffs. The outboard end of the cuff connects to the yoke and the blade root. The blades are modified Model 412 blades with nearly 5 feet removed from the inboard end and metallic plates bonded to the upper and lower surfaces to provide the hub attachment. These blade modifications resulted in a bulky and aerodynamically "dirty" yoke/cuff/blade attachment area, but it served the purpose for the hub concept evaluation.

The component of interest is the yoke. Each arm is able to accommodate a pitch change in excess of 35° in each direction. At the same time, the yoke carries the blade centrifugal and lifting forces, transmits engine torque, and allows flapping and lead-lag motions. These functions of the yoke are obtained by discrete tailoring of the dynamic and structural cross-section properties. This is realized by a series of filament-wound fiberglass/epoxy belts, shown in figure 1-4. These belts are interleaved in a closed-cavity tool, shown in figure 1-5, that molds the yokes. Additional off-axis plies of fiberglass/epoxy tape are added in the mast attachment area and taper out as necessary to support the shear-restraint pivot and shape the flapping portion of the yoke.

YOKE STRUCTURAL TECHNOLOGY

Full-scale fatigue tests of complete rotor hub assemblies were conducted to evaluate the structural integrity of the design and to support the experimental flight tests. A hub assembly was subjected to about 275 percent of the maximum level flight oscillatory loads. Delaminations beginning at the corners of adjacent arms of the yoke were induced early during the testing, but the test was continued at that load level for a sufficient number of cycles to demonstrate the fail-safe features of the design. At the conclusion of the test, no significant loss in stiffness could be detected. The original Model 680 yoke that was flight tested was flown throughout the entire flight envelope and at high-g maneuvers without any problems.

To better understand and improve the delamination character-
istics of the yoke, an extensive analysis and a series of coupon
and component tests were performed. A finite element model of
the corner area was made (fig. 1-6). The analysis showed that
the large corner radius, which would be beneficial in a metal
structure, is actually detrimental in a composite structure.
This is because of the large number of ply terminations required
to form the corner. The analysis was expanded to the flapping
flexure portion of the yoke to explore opportunities to improve
the delamination strength in this area (fig. 1-7). The analysis
also considered the consequences of manufacturing improvements
such as fewer and thicker belts of the unidirectional rovings
and fewer off-axis plies of tape. The results of this analyti-
cal study and design support coupon tests showed that better
management of Poisson's ratio mismatch by special ply sequencing
between the belts would significantly improve the interlaminar
stresses and the delamination strength. It was also found that
a slight resculpturing of the outer flapping flexure contour
would also reduce the overall surface fiber stresses. The
improvements were incorporated in a second-generation Model 680
yoke, shown in figure 1-8, that was also evaluated in the
fatigue test machine. The delamination problem in the corners
was eliminated and the test loads were periodically elevated
until the next delamination mode was found. This occurred at an
outboard location in the flapping flexure of the yoke. This new
delamination mode is also fail-safe and provides approximately
70 percent of additional load ability over the original design,
which is well above the maximum flight loads.

An analysis performed on the area of the delamination showed
that it was initiated by an interlaminar stress concentration at
a free edge. Bell has conducted research on this problem and
has developed an innovative adhesive inner-layer concept for
delamination arrestment. This concept is shown in figure 1-9.
The key point is to use a high-strain ductile adhesive layer at
the critical interfaces at the free edge. This changes the
initial delamination mode from a brittle fracture to a more duc-
tile fracture. Proper positioning of the adhesive layers
results in a reduced interlaminar normal stress distribution
through the thickness of a given laminate under a given load, as
shown in figure 1-10. Numerous coupon tests have verified this
approach. Figure 1-11 shows that the static delamination
strength of coupon test specimens with adhesive layers is nearly
double that of specimens without adhesive layers. Dynamic
improvements have also been found in fatigue test coupons. An
interesting aspect of this technology is that the adhesive layer
acts as a buffer between critical plies. This buffer tends to
delay the propagation of transverse cracks to adjacent plies,
which would then develop into a delamination between those
plies. This can be seen in the photomicrograph of the edge of a
coupon in figure 1-12. This concept has been applied to the
yoke and will be tested in the near future. The analysis shows
that an additional 20 percent of load ability can be realized
for this design.

MODEL 680 FLIGHT TEST RESULTS

In May 1982 the first flight of the Model 680 rotor system on a Bell Model 222 aircraft was made (fig. 1-13). Some of its accomplishments are listed below:

(1) Nearly 600 flight-hours

(2) Split "S" maneuvers with dives exceeding 210 knots

(3) 2.8g to -0.1g maneuvers routinely performed

(4) Demonstration rides for over 1000 people

(5) No rotor limitations

In addition to successfully demonstrating the manufacturing, structural, and stability aspects, thus making it possible to realize the direct benefits of a bearingless rotor system, the Model 680 rotor system has also displayed excellent handling qualities and vibration characteristics.

The Model 680 was flown on the Model 222 helicopter without a stability augmentation system. The gust penetration and control response were excellent. There was no tendency for the nose to tuck under during a pushover or pitch up in turbulence, so there was no corrective action required by the pilot. During low-g maneuvers, there were no noticeable trim changes in lateral cyclic. Control coupling was in harmony throughout the flight regime. All of the indications are that this system could be FAA certified for single pilot IFR conditions without a stability augmentation system. These features are the result of the well-defined rotor kinematics, isolated rotor stability, and low-vibration aspects that the rotor system possesses.

The most noticeable and outstanding feature of the Model 680 rotor system is the very low vibration level throughout the cabin under all flight conditions, including extreme maneuvers. A summary of the cabin vibrations in all seats, all directions, all gross weights, all centers-of-gravity, and all altitudes of the Model 680 rotor with two LIVE units is presented in figure 1-14. The LIVE units lower the vibration levels primarily at transition where the vertical excitations are the largest. The hundreds of data points represented in this figure demonstrate the consistently good vibrations resulting from the rotor dynamics that have been experienced by hundreds of passengers.

These excellent dynamics represent the "nodalized rotor technology" at Bell. This technology concept goes beyond rotor natural frequency placement to nulling the potential hub shear and moment excitations from the rotor by tailoring the blade mode shapes. This patented concept has three key elements:

(1) Low-mass, high-stiffness hub

(2) Concentration of mass at an inboard blade location (further inboard than that for conventional frequency placement)

(3) Discrete blade stiffness

These ingredients are all found in the bearingless rotor concept and exploited in the Model 680 rotor design. A series of model tests has also verified this technology.

The outer contour of the pitch change cuffs serves as a fairing that reduces the drag coefficient for most of the hub. Even though the bearingless hub has a greater radial extent, the parasitic drag was found to be less than that of conventional rotor hubs. The radial location of the hub/blade attachment area caused a profile power loss that was observed in hover and at minimum power forward flight. Subsequent testing with temporary fairings showed that the profile power loss could be recovered. Wind tunnel hub drag tests have also shown that the parasitic drag could be further reduced with refinements in the cuff geometry.

ADVANCED LIGHT ROTOR

The use of the modified Model 412 blades meant that the aerodynamics were not optimum because of the "dirtiness" of the hub/ blade attachment area and the radial distribution of airfoils that had been optimized for the Model 412 radial locations and rotational speeds. However, with the successful demonstration of all the other features of the Model 680 rotor system, the time had come to integrate advanced aerodynamic technology with new rotor blades optimized for application with the rotor hub. Bell also took this opportunity to employ an innovative plastic tooling concept to minimize the tooling costs and lead time. These new rotor blades for the Model 680 hub are called the Advanced Light Rotor (ALR).

Four unique airfoils with different thicknesses were developed for the ALR blades. These airfoils were tailored for their specific aerodynamic environments along the rotor blade span and optimized for best lift, drag, drag divergence Mach number, pitching moment, and lift-to-drag ratio where it is most advantageous. Also, the pitch change cuffs were made integral with the blades. The integral cuff design reduces the weight and size of the hub-to-blade interface and provides a smooth transition from the elliptical cross section of the inboard cuff to the first tailored airfoil. The ALR blades also incorporate the nodalized rotor technology of mass and stiffness tailoring. The tooling is shown in figure 1-15. The ALR blades with the Model 680 rotor hub installed on the test aircraft are shown in figure 1-16. At this writing, the flight testing has just begun. The aeromechanical stability has been verified and the vibrations

are as good as the original Model 680 rotor system. Envelope expansion and performance flights are underway.

ADVANCED ROTOR TECHNOLOGY IMPLEMENTATION

The next application of Bell's advanced rotor technology is a bearingless main rotor for helicopters in the 14,000- to 18,000- pound class. This larger rotor system employs the basic Model 680 concept with enhancements and considerations applicable to a rotor system of this size. The new rotor system is shown in figure 1-17. One major difference is that there are two yokes, one for each opposing pair of blades, to minimize tooling costs and size. Another major difference is that there are separate yoke-to-cuff and cuff-to-blade attachment joints to provide manual fold ability, reduce the thickness of the cuff and blade root, and simplify blade root construction. Removable fairings for this area were designed to provide a smooth surface over the cuff and blade cutouts, which are necessary for folding clearances. The advanced structural concepts, hub dynamics, tailored airfoils, and nodalized rotor technologies are all incorporated in the large bearingless rotor design. This rotor system will be first demonstrated on an AH-1W helicopter in late 1987 (fig. 1-18).

The advanced bearingless rotor will expand the mission potential of the AH-1W helicopter. Direct benefits in reliability, maintainability, vibration, and handling qualities will provide lower cost of ownership, reduced crew fatique, and improved performance of avionics and armament systems. The composite hub and blades were designed to have greatly improved ballistic survivability. The positive and negative g maneuver envelopes will be expanded with the rigid rotor. The aerodynamic improvements will provide over 1000 pounds more payload, 20 knots more speed, greater vertical rate of climb, and increased hover altitude. All of these features will not only enable the AH-1W to better perform its current missions, they will also enable the helicopter to execute multimission roles and dedicated air-to-air combat with alternate fire control and weapons systems.

Other spinoffs from Bell's advanced rotor technology include four U.S. government contracts to further explore various aspects, the foundation for the LHX rotor system, and confidence to apply a bearingless main rotor system to the next generation of Bell's helicopter products.

PART II. METHODOLOGY DEVELOPMENT

The importance and complexity of analytical development and design application in the field of aeromechanics have been widely recognized in the rotorcraft community. New developments in the methodologies of aerodynamic performance, airloads, rotor vibratory loads, aeromechanical stability, aircraft vibration,

and handling qualities, among others, are presented each year at the AHS National Forum and specialists' meetings. The following discussion concentrates on some of the recent accomplishments at Bell in the field of aeromechanics methodology. Specific emphasis is given to analytical tool development, correlation studies, and design applications as they relate to advanced design requirements.

AERODYNAMICS

Airfoil Design

Bell uses a system called Aerodynamic Design and Analysis Methodology, or ADAM, in the design of its advanced airfoils. The ADAM system's inverse design capability is used to develop airfoils with aerodynamic properties that will satisfy partic- ular performance requirements. The V-22 airfoils were designed using this system. Figure 2-1 shows the maximum lift coeffi- cient at Mach 0.4 and the drag divergence Mach number at a lift coefficient of zero for several Bell airfoil sections, including those for the V-22. For comparison purposes, the NACA 64 series of airfoils used in the XV-15 rotor are also shown.

The advanced airfoils developed at Bell in recent years have met their design objectives. The V-22 tilt rotor airfoil designs are used as an example. The V-22 aerodynamic design objectives and priorities are shown in figure 2-2. In comparison with the XV-15, the following aerodynamic goals were to be achieved:

    (1) Improved maneuverability in helicopter mode at 40 knots.

    (2) The same low-drag characteristics at 300 KTAS at 20,000 feet, cruise, as in the XV-15.

    (3) No compressible divergence drag up to 350 KTAS at 20,000 feet, cruise.

    (4) High lift/drag ratio for hover efficiency.

The basic airfoil design requirements called for a set of four airfoils, one each at the 0.25, 0.5, 0.75, and 1.0 blade radial stations (r/R). Contraints on the thickness and maximum pitching moment were also imposed on the design. These are shown in figure 2-2.

As an example of the results of the ADAM system's inverse design capability, the 12-percent thick V-22 airfoil (XN12 in figure 2-1) will be evaluated here. After an extensive theoretical evaluation of the new section, wind tunnel tests of the airfoil were conducted in the Boeing Supersonic Wind Tunnel (BSWT) facility. The measured data shown in figure 2-3 were obtained from the BSWT. Also shown in the figure are the design objectives. The data indicate that all goals were met except the cruise drag coefficient C_d at $C_\ell = 0.2$ and $M = 0.65$.

The XN12 airfoil was also previously tested in the United Technology Research Center (UTRC) wind tunnel for Advanced Technology Blade (ATB) evaluation. Comparisons of the XN12 data from the UTRC tunnel with those from the BSWT indicate that the UTRC results are slightly lower in $C_{\ell\,max}$ (e.g., $\Delta C_\ell = 0.1$ at $M = 0.4$), C_d, C_{m_o}, and L/D. For the XN-12 at $C_\ell = 0.2$ and $M = 0.65$, a drag coefficient of 0.00535 was measured in the UTRC tunnel (shown in figure 2-3). Since the design goal of $C_d = 0.006$ falls between the data from the two wind tunnels, it is believed that the designed XN-12 airfoil satisfies the low-drag requirement and closely meets the other design objectives.

Transonic Blade Design

Three-dimensional transonic flow codes are being developed in the technical community that determine the potential flow pressure distribution about arbitrary blade configurations. However, in order to determine the torque difference between two different blades, an evaluation of the viscous effects must be included. An approach to this problem being pursued at Bell is to couple a boundary layer routine with the potential flow routines. This produces a drag and torque distribution over the blade due to viscous effects. In addition, the displaced blade surface can be evaluated in the potential flow code to determine those changes in the flow field solution due to boundary layer displacement. This method can be used to develop blade tip shapes that minimize the advancing blade drag and eliminate shock-induced separation.

Figure 2-4 shows, for comparison, the measured pressure distribution on the OLS blade, a theoretical two-dimensional airfoil result, a theoretical three-dimensional potential flow solution, and the theoretical three-dimensional flow results after a boundary layer was added. Data show that the two-dimensional results greatly overpredict the shock strength. The three-dimensional potential flow code calculates a much more realistic pressure distribution for this case. However, the drag calculated from this analysis is very low, since the forward displaced sonic zone produces a leading edge suction. This type of result from the potential flow codes leads to erroneous conclusions when comparing the torque calculations of different tip shapes. The pressure distribution with the displaced boundary layer surface is only slightly changed from the potential solution. However, the drag from this analysis, including the effect of additional boundary layer growth due to the forward displaced shock wave, is more useful than the pressure distribution in the evaluation of an advancing blade performance at high tip Mach numbers.

Rotor Lateral Flapping at Low Advance Ratio

The significance of fore and aft nonuniformity in rotor inflow to rotor lateral flapping at low advance ratio was identified by

Harris (ref. 1). Work presented in references 2 and 3 suggest that at low advance ratios, it is necessary to use a free wake geometry calculation to achieve a desired correlation in rotor lateral flapping. Reference 2 also states that the calculated values of the flapping motion are sensitive to details of the wake structure, especially the viscous core radius of the tip vortices.

A recent attempt in the correlation of rotor lateral flapping was conducted at Bell using a simplified nonuniform inflow representation in C81. The math model can be stated as

$$v_i = \frac{4}{3} \, \bar{v}_i \, \chi \, (1 + K \cos \psi) + \text{tip vortex effects}$$

where $\bar{v}_i$ is the average value of the induced velocity across the disc as determined from momentum theory, χ is the nondimensional blade station (0 = root, 1 = tip), ψ is the blade azimuthal position (0 when blade is over the tailboom), and K is the nonuniform inflow parameter. K is a function of the advance ratio as depicted in figure 2-5.

Correlations in rotor flapping and rotor power were conducted using the data computed by the simplified C81 nonuniform inflow analytical model and those measured by Harris in reference 1. The results are shown in figures 2-6 through 2-8. Shown also are the analytical data calculated using the C81 uniform inflow model. For comparison, analytical data from CAMRAD with uniform inflow, undistorted wake, and free wake models are also presented. In these calculations, a delta drag coefficient of 0.006 was added to the baseline V23010-1.68 airfoil data table to account for the Reynolds number effect.

Figure 2-9 presents the induced velocities along the rotor's longitudinal axis, calculated with C81 and CAMRAD at an advance ratio of 0.08. It is seen that though the C81-computed induced-velocity distribution does not compare directly with that of the CAMRAD, the resultant effect on the lateral flapping is in close agreement. This is apparent when one refers to the equation (7) in reference 1.

The results in figures 2-6 through 2-8 indicate that the C81 simplified nonuniform inflow model is as good as the CAMRAD free wake model in predicting rotor lateral flapping at low advance ratios, that the rotor power predicted with the C81 uniform inflow correlates with the test data, and that the C81 nonuniform inflow model underpredicts the rotor power required by 7 percent.

Tilt Rotor Aerodynamic Performance

The primary methodologies used to analyze and predict the aerodynamic performance of tilt rotors in the hover and axial flow

states are AR7906 (hover) and its derivative AR7907 (axial flow). These computerized methodologies are based on a blade element rotor model using lifting surface theory and a circulation-coupled prescribed wake. These performance programs apply to a wide variety of rotors, ranging from the low disk loading, low-twist helicopter rotor to the high disk loading, high-twist rotor of the tilt rotor aircraft. A correlation of calculated and measured performance for the XV-15 tilt rotor is shown in figure 2-10 for hover and figure 2-11 for axial flow (i.e., propeller mode).

The performance methodology applied to the tilt rotor forward flight in conversion modes is ARAM46. ARAM46 is also based on a blade-element model that includes unsteady and three-dimensional aerodynamics. A correlation of the calculated results with test data for an isolated proprotor is shown in figure 2-12.

Panel Method Pressure Calculations and Correlations

Three-dimensional panel methods are being used at Bell to distribute the aerodynamic loads on new vehicles. This is being done in order to produce as accurate a load distribution as possible so that the minimum weight structure can be developed. At the present time these panel codes represent the most versatile and efficient approach to solve for the aerodynamic loads about complicated configurations at low Mach number.

Panel code validation. - In order to gain experience in the use of the three-dimensional panel method results, several correlations between calculated and measured airload distributions have been conducted. Some examples of these correlations are presented here.

Figure 2-13 shows the V-22 wing cross section with its flap deflected 30°. As can be seen, this is a very complicated geometry that is difficult to model because of element interference and flow separation. In figure 2-13 the calculated pressure distribution on this configuration is compared to the measured pressure distribution. The VASAERO (ref. 4) panel modeling used in this case included boundary layer calculations, the wake models for the separation location on the flap, and the wake of the main wing. To simulate a two-dimensional flow field, the main wing for the panel model had an aspect ratio of 30 whereas the aspect ratio of the actual V-22 wing is 5.5. As can be seen, the theoretical results compare with the measured values quite well for this case.

Figure 2-14 depicts the measured and calculated pressure distribution along the V-22 spinner. In this case the pressure distributions correlate very well for the clean spinner case. It should be noted that no effort has been made so far to model the blade holes, blade root end, and eyebrows using a panel method. A comparison of the VSAERO panel results and measured pressures at station 359.9 on the nacelle of the V-22 is given

in figure 2-15. It shows that the panel method results are reasonably good, even over this complicated shape.

As part of the V-22 inlet design studies, a VSAERO panel model was generated to evaluate the internal flow characteristics of candidate geometric configurations. This model was iteratively modified to eliminate external flow separation on the inlet at critical flight conditions. An essentially separation-free design was necessary to achieve the inlet head loss and distortion goals established for the V-22 inlet. A wind tunnel test program was conducted to measure the performance of the configuration selected. The model represented the right hand engine nacelle and stub wing of the V-22 at 0.4 scale. A comparison of the calculated and measured static pressure distribution in helicopter mode from this test is shown in figure 2-16. The agreement between the predicted and measured results is remarkable, considering the complexity of the configuration. Equally good agreement was obtained for the transition and cruise flight modes.

Air loads distributions. - Because of the excellent results produced in these and other VSAERO correlations, this code is being used to distribute the air loads on the V-22 airframe. Accurate air load distributions are required to minimize the structural weight of the vehicle.

The V-22 airframe model was used to determine the downwash angle and total lift of the empennage. The Generic Tilt Rotor (GTR) simulation program was used to fly maneuvers to determine the most critical total point load conditions. At these conditions the VSAERO code was used to determine the distributed air loads for input into the NASTRAN structural analysis program. A LOADS component of the ADAM system is being developed to automate this process. A preliminary beam bending moment distribution on the empennage from the VSAERO pressure distribution produced by ADAM/LOADS for this case is given in figure 2-17. It shows the kind of results that may be produced for complicated three-dimensional configurations and applied to structures design.

DYNAMICS

Nodalized Rotor

The vibration characteristics of the four-bladed hingeless rotor exhibit high 4/rev vibrations in a low-speed transition regime because of blade-vortex interaction. As airspeed increases from the transition flight, the 4/rev vibration level first decreases, then increases again as the helicopter flies faster. The primary excitation forces are the hub 4/rev vertical shear and the hub 4/rev pitching and rolling moments. The sources of the hub 4/rev vertical shear and 4/rev moments are the blade root 4/rev vertical shear and the 3 and 5/rev beamwise bending moments, respectively. Therefore, it is feasible to achieve the desired low 4/rev airframe vibration by minimizing the blade

response in the 3/rev, 4/rev, and 5/rev harmonic components. Bell's nodalized rotor technology approach is to judiciously tailor rotor structural and aerodynamics properties in such a way that inertial loads cancel out blade aerodynamic loading at rotor hub, forming a nodal point.

The methodology of the nodalized rotor leads to the following specific design features:

(1) An extremely stiff and lightweight hub.

(2) A large concentration of mass near the 40-percent blade radius.

(3) A reduction in mass in the outboard 30 percent of the blade.

(4) An increased beamwise and chordwise stiffness for the entire blade.

An analytical prediction of the benefit of the nodalized rotor over a conventional design indicated a 40- to 45-percent reduction in hub loads in the low-speed transition. (The conventional design referred to here is a rotor design achieved using the conventional frequency separation criteria.) To validate the analytical prediction, one-fifth scale aeroelastic models with an NACA 0012 airfoil and a constant chord were fabricated for both the conventional design and the nodalized rotor. The models were then tested in identical back-to-back flight conditions in the LTV low-speed wind tunnel. Comparisons of measured and predicted hub loads versus the tunnel speed (plotted in units full-scale speed) are presented in figure 2-18. The results indicate that the predicted reduction in hub loads is conservative.

To further explore the nodalized rotor concept, a model rotor was designed and fabricated with advanced airfoils and highly tapered planform blade. This effort is being conducted under a NASA-Army contract. The thrust-weighted chord of the tapered blade is equal to the constant-chord 0012 airfoil blade tested earlier. The predicted hub loads of the aerodynamically optimized nodalized rotor are also shown in figure 2-18. The weight penalty of the aero optimized nodalized rotor versus the conventional design is about 0.3 percent of the gross weight. Wind tunnel testing of the aero optimized nodalized rotor will be conducted in the NASA-Langley Transonic Dynamics Tunnel (TDT) in March 1987. The two models previously tested in the LTV low-speed wind tunnel will also be tested in the TDT for comparison purposes.

Tilt Rotor Loads

The aerodynamic interference between the wing and tilt rotor blades is the primary source of the oscillatory blade and hub

loads. For tilt rotors with three-bladed gimbaled hubs, such as the XV-15 and V-22, the aerodynamic interference between the wing and rotor is responsible for the high 2/rev and 3/rev blade beam loads, 2/rev and 4/rev blade chord loads, and the 3/rev hub in-plane shears in the airplane cruise mode. The flow field of the wing is approximated in Bell's computer program DYN5 (ref. 5) and recently in C81 by superimposing the flow field of an elliptical profile at zero angle-of-attack on that of a flat plate representing the wing angle-of-attack (figs. 2-19 and 2-20). The ellipse simulates the wing thickness while the flat plate represents the circulation. The interference is assumed to be zero on the outboard half of the rotor disk (away from the wing, i.e., 0 < azimuth < 180°).

To analyze the aerodynamic interference between the proprotor and fuselage more sophisticatedly, the panel method, computer program VSAERO (ref. 4), was used to calculate the change in flow field around a blade element due to the presence of the wing, spinner, nacelle, or fuselage. Changes in the flow field for blade elements due to the presence of the airframe were calculated using VSAERO and the DYN5 simplified analytical model. Results are compared in figure 2-21. Good agreement is evident between the two analytical approaches near the 270° azimuthal position (when the reference blade is positioned right in front of the wing). The differences between the two analyses are due to the assumptions made in the simplified model that any aerodynamic interference on the outboard half of the rotor disk is neglected and that flow blockage, other than by the wing, is not included.

The VSAERO-calculated change in the flow field was input to the C81 computer program using a table look-up. This analytical approach (C81/VSAERO) was used to predict the V-22 rotor loads in the cruise airplane mode. Figures 2-22 and 2-23 show comparisons of computed and measured blade loads in the first four harmonic components. Without the aerodynamic interference representation (data not shown), the correlation of the 1/rev is still good, but the computed higher harmonic components are nearly zero. Using the DYN5 flow approximation method, good correlations (data not shown) are achieved in the 1/rev and 2/rev components, but not so good correlations are observed in the 3/rev and 4/rev components. A harmonic analysis of the change in the blade angle-of-attack (fig. 2-21) due to the aerodynamic interference reveals that the VSAERO data consist of 2/rev, 3/rev, and 4/rev values of 0.79°, 0.54°, and 0.36°, respectively. The corresponding results from the DYN5 data are 0.70°, 0.41°, and 0.19°, respectively. It is seen that the simplified analytical model does well for the 2/rev. It is, however, not adequate for 3/rev and 4/rev blade load predictions.

The C81/VSAERO methodology was used to predict the V-22 3/rev hub in-plane shears and the results are presented in figure 2-24. The V-22 3/rev hub in-plane shears were also inferred using

the pylon vibrations and transfer functions measured on the 0.2-scale aeroelastic model. The hub loads from the inferred method seem to agree quite well, both in trend and in magnitude, with those predicted by the theory.

Tilt Rotor Wing/Pylon Dynamics

The accuracy of a dynamic analysis of the wing, pylon, and pylon support structure is critical to not only cabin vibrations but also to oscillatory loads and proprotor stability. MSC/NASTRAN Version 63 was used to perform the dynamic analyses. To validate the modeling methodology for the V-22, a full-scale wingtip box test was conducted (ref. 6). The test specimen consisted of an 8-foot span from the outboard end of the V-22 wing, and included a mass-simulated pylon, and an actual pylon support structure. Prior to the vibration test, stiffness tests and measurements of mass and inertia properties were conducted. The measured stiffness and inertia properties were then used in the posttest analysis. Figures 2-25 and 2-26 show, for comparison, measured frequencies along with those of pretest and posttest analyses. The results indicate that the finite element model is proper, as evidenced by the pretest analysis, and that the current structural dynamics modeling of the wing/pylon structure is adequate for the in-flight wing/pylon modes prediction.

Proprotor Stability

Proprotor stability has been investigated at Bell since the 1960's. Linear and nonlinear analyses (DYN4 and DYN5) have been developed and wind tunnel tests of scaled aeroelastic models have been conducted. Extensive experience in correlation has been acquired. To aid in modeling a proprotor with a coning flexure, such as the V-22 design, an eigenvalue analysis was recently developed (ref. 7). The analysis is called ASAP (Aeroelastic Stability Analysis of Proprotors). The ASAP analysis models a modal airframe, an elastic rotor on a gimbaled hub with flapping, coning and lead-lag motions, and a lumped parameter drive system. The airframe modal parameters are calculated using the NASTRAN finite element dynamics model. A general automatic flight control system (AFCS) is also included. The blade aerodynamics can employ either the 3/4 radius approach or two-dimensional blade element theory. The airframe aerodynamics include airframe force and moment nondimensional derivatives and control surface deflection force and moment nondimensional derivatives so that control inputs from the SCAS will generate forces and moments on the rigid body and elastic modes of the airframe.

The application of the ASAP computer codes to proprotor stability was validated using the stability data measured on the V-22 0.2-scale semi-span aeroelastic model. Figure 2-27 shows the correlation of wing beam and wing chord damping in percent critical versus the airspeed. The degree of correlation is satisfactory.

HANDLING QUALITIES

Rotorcraft Frequency-Domain Identification

Many criteria in the recently updated helicopter handling
qualities specification (ADS 33) are based on transfer function
parameters derived from linear models of the aircraft. To
demonstrate compliance with these criteria requires flight test
generated frequency response data. This is a new requirement
for the rotorcraft community. The Army (ref. 8) has demon-
strated the practicality of producing the data and has developed
data-reduction algorithms that not only fit the raw data but
also identify the equivalent parameters of the transfer function
represented by the data.

To gain experience in these techniques, some recent flight tests
of the Model 222/680 helicopter were devoted to generating
frequency response data. Data were taken for cyclic and pedal
inputs at several forward flight speeds in the 80 to 125 KTAS
range. Sinusoids at various frequencies were input through the
roll, pitch, and yaw SCAS actuators, as appropriate, with the
aircraft trimmed at the desired speed and without pilot control
inputs. Where possible the sine wave amplitudes were adjusted
until the resulting aircraft attitude oscillation was approxi-
mately ±7.5° in the driven axis. Good data were obtained in the
0.5 rad/sec to 8-10 rad/sec range. Below 0.5 rad/sec the input
periods became too long and the aircraft changed trim state
before an adequate data sample could be collected. Above 8-10
rad/sec aircraft response became too small to record, even with
the SCAS actuator operating at full authority. For handling
qualities the 8-10 rad/sec limitation may not be a problem,
since most of the interesting characteristics reside at lower
frequencies. The 0.5 rad/sec limitation does preclude identi-
fication of some important low-frequency characteristics such as
the phugoid and spiral modes. Therein lies a topic of interest
for future development of this technique at Bell.

The frequency response data were subsequently compared with
equivalent C81 results for the Model 222/680. This provided a
check on the accuracy of computed frequency responses based on
the transfer function parameters calculated by C81. Typical
results are shown in figure 2-28. The measured gains are
matched quite well by the computed gain response. The same is
not true for the phase response. If, however, we draw on
reference 8 and related fixed-wing experience (ref. 9), which
justify the inclusion of the e^{-Ts} or pure delay term in the
numerator of the calculated transfer function to account for
high-frequency and unmodeled or nonlinear effects, the phase
responses come into better agreement. In this case it was found
that an equivalent pure delay of 145 milliseconds was necessary
to correlate the data. With this modification the estimated
transfer function for the sample case becomes:

$$\frac{\theta}{\delta_{F/A}} = \frac{0.99\, e^{-0.145s}\,(s + 0.07)(s + 0.82)}{\left[s^2 + 2\,(0.14)\,(0.25)\,s + 0.25^2\right]\left[s^2 + 2(0.82)\,(1.75)s + 1.75^2\right]}$$

where all parameters except $e^{-0.145s}$ were determined by C81.

As driven by ADS 33 and the success of this preliminary effort, Bell will continue to evolve its capability in the techniques of in-flight frequency responses and application of these data for specification compliance and math model refinement.

Tilt Rotor Airplane Mode High-g Maneuvers

The capability of C81 to predict high-g maneuvers for tilt rotors in airplane mode was recently validated. The validation was based on a correlation with measured XV-15 flight test data. The measured data were recorded during flight 290, counter 1014, of XV-15 Ship 702. The aircraft entered the maneuver at 216 KIAS by initiating a right roll with SCAS on. The bank angle change was 82° in 2.5 seconds. During the course of the roll, aft stick was applied, generating a peak pitching rate of 40 deg/sec. The control applications resulted in a 4.2g load factor at 214 KIAS. A total of 40 seconds of data was taken during the maneuver, and the 20 seconds of data where the peak load factor occurred are shown in figure 2-29.

The C81 analytical model includes aerodynamic descriptive data for the rotors, wings, fuselage, and aerodynamic surfaces. The dynamics of the rotors were modeled through a modal representation with 10 elastic modes. The analysis was performed with SCAS off. The pilot control inputs in C81 were adjusted to reflect the control surface deflections due to pilot stick inputs and the SCAS effect. Computer simulation was limited to 10 seconds near the time when the maximum load factor occurred. The analytical data are also presented in figure 2-29 for comparison.

The results indicate that the peak load factor is predicted within 0.2g and that the predicted roll rates and roll attitudes are within 4 deg/sec and 4°, respectively. Correlations in pitch rates and pitch attitudes are good. The peak transient loads of the blade and the pitch link of the right rotor (not shown in figure 2-29) are predicted with a maximum discrepancy of 10 percent.

CONCLUDING REMARKS

The thrust of the activities described in this paper is to provide adequate methodologies so that the development of advanced military rotorcraft can be undertaken with a minimum risk. As indicated, some progress has been made in achieving this goal, but the challenge has by no means been met. Bell

fully recognizes and appreciates the extent of the challenge and has committed to continue the development of the aeromechanics methodology.

REFERENCES

1. Harris, F. D.: Articulated Rotor Blade Flapping Motion at Low Advance Ratio. Journal of the American Helicopter Society, vol. 17, no. 1, Jan. 1972.

2. Johnson, W.: Comparison of Calculated and Measured Helicopter Rotor Lateral Flapping Angles. Journal of the American Helicopter Society, vol. 26, no. 2, April 1981.

3. Johnson, W.: Assessment of Aerodynamic Models in a Comprehensive Analysis for Rotorcraft. NASA TM 86835, October 1985.

4. Maskew, B.: Program VSAERO, A Computer Program for Calculating the Nonlinear Aerodynamic Characteristics of Arbitrary Configurations: User Manual. (Prepared for NASA Ames Research Center, Moffett Field, CA., under Contract NAS2-8788.) April 1982.

5. Yen, J. G.; Weber, G. E.; and Gaffey, T. M.: A Study of Folding Proprotor VTOL Aircraft Dynamics, Volume 1. AFFDL-TR-71-7, September 1971.

6. Sprangers, C.A.; and Stevenson, M. K.: Results of the V-22 Preliminary Design Wing Test Program. Paper presented at the 42nd Annual Forum of the AHS, June 1986.

7. Hsieh, P. Y; Levenson, W.; and Parham, T.: Aeroelastic Stability Analysis of Proprotors (ASAP). BHTI Report 301-909-003, July 1986.

8. Tischler, M.; Leung, J.; and Dugan, D.: Identification and Verification of Frequency Domain Models for XV-15 Tilt Rotor Aircraft Dynamics. NASA TM 86009, August 1984.

9. Hoh, R.; et al.: Proposed MIL Standard and Handbook - Flying Qualities of Air Vehicles, Volume II: Proposed MIL Handbook. AFWAL-TR-82-3081, November 1982.

PART III. ADVANCED CONFIGURATION STUDIES AND HARDWARE DEVELOPMENT

Part III presents some results of advanced tilt rotor configuration studies conducted by the Preliminary Design group at Bell. The first section discusses concept evaluation of military and commercial configurations of manned aircraft. The second section presents an idea for an unmanned tilt rotor for shipboard operation and describes a prototype development program being performed by the predesign groups of Bell and their tilt rotor partner, Boeing Vertol, to build and demonstrate a 500-pound gross weight tilt rotor unmanned aerial vehicle for use by the military forces of the U.S. and friendly allies.

MILITARY AND COMMERCIAL CONCEPTS

V-22 Derivatives

The V-22 Joint Services Vertical Lift Aircraft (fig. 3-1) is well along in its full-scale development, with first flight scheduled for mid 1988. The V-22 is an unarmed utility/ transport aircraft designed as a Marine assault vehicle. It is equipped for shipboard operation and incorporates a folding wing and rotors and a fuselage with an aft loading ramp to facilitate loading and unloading. The fuselage and cockpit are unpressurized.

The first derivative application of the V-22 is for antisubmarine warfare (ASW) missions. Figure 3-2 illustrates the V-22 ASW configuration concept. Search equipment includes expendable sonobuoys, onboard processing, FLIR, radar, and ESM. A magnetic anomaly detector and dipping sonar are used for localization. The V-22 ASW has the ability to soft deploy and monitor large acoustic sensors for screening purposes, and because of its ability to hover and fly at low speeds in the helicopter mode, it can retrieve advanced sophisticated sensors for redeployment. The high cruise speed and ability to operate from a variety of decks are also a significant advantage. The aircraft carries up to four torpedoes or antisurface missiles.

Because the basic V-22 carries no weapons, an armed escort aircraft with similar flight performance is needed. Obviously a helicopter would be too slow, and typical fighters are too fast. The simplest solution is a modified V-22 with counter air weapon systems adapted as shown in figure 3-3. Since the V-22 was optimized for other applications, it does not present the best configuration for an air-to-air combat aircraft. A smaller aircraft might be more suitable for this mission. Although weight fraction trends are adverse for a smaller aircraft, its reduced target size and increased agility offset the penalty. Figures 3-4 and 3-5 show two alternative configurations for a V-22 escort. The performance of these aircraft is closely matched to the V-22.

The next V-22 derivative is a commercial version with minimum change (fig. 3-6). Obviously, some of the military requirements - such as IR suppressors, bladder tanks, and wing and rotor folding - would be eliminated to reduce cost and weight. A commercial derivative could carry up to 31 passengers and enough fuel for up to 600 miles. One of its primary uses might be as a light cargo transport for overnight package express.

Commercial Applications

Three possible tilt rotor configurations have been developed for the specific requirements of commercial operations. The driver in commercial applications is productivity, which, by definition, demands optimization of performance and cost. A cleaner shape for lower drag and the maximum payload for a given gross weight are primary factors in productivity.

Trade-off studies were conducted on the three configurations. The first configuration resembles the XV-15 in that a high wing placement is used with tilt nacelles and an "H" tail (fig. 3-7). The second configuration relocates the wing at the bottom of the fuselage (fig. 3-8). Although interference drag is slightly greater with the low wing placement, overall drag is reduced because the wing spars can now pass through the belly below the cabin floor, allowing an unrestricted cabin height and minimum fuselage profile. The low wing also allows retraction of the landing gear into the wing roots, eliminating the need for sponsons. The "T" tail configuration reduces interference drag by minimizing the number of surface intersections.

The third configuration, a somewhat more radical departure from convention, is a low-wing, fixed-engine aircraft with a canard surface forward and twin fins aft (fig. 3-9). Use of the canard to carry approximately 20 percent of the weight of the aircraft accomplishes several things. First, it reduces the wing area and, hence, the rotor download during hover. This in turn minimizes the installed power requirements, yielding a lower empty weight. The lifting canard also allows a more favorable cg placement ahead of the leading edge of the wing root. This position more closely approximates the cg position during hover, resulting in less cg shift from hover to cruise flight. Reduced cg travel minimizes hub stiffness requirements and provides indiscriminate loading. The lifting control surface reduces the total lift in cruise, minimizing the induced-drag penalty. The usual objections to a canard include the difficulty of handling during landing, but since takeoff and landing of the tilt rotor are done in the helicopter mode, the canard has no effect on that flight regime.

The three configurations were sized for a gross weight of 20,000 pounds and then evaluated parametrically for drag and empty weight. A comparison of the three aircraft reveals that the canard is the best configuration from the standpoint of both drag and weight, as shown below:

Configuration	Empty Weight (lb)	Drag (ft²)
High wing, H-tail	15,407	12.1
Low wing, T-tail	15,109	10.1
Low wing, canard	14,834	8.7

Additional variants of the canard configuration have also been studied. Figure 3-10 shows an interesting executive transport that uses a highly swept midwing configuration. This aircraft, having a compact pressurized fuselage like a Lear jet, accommodates the wing carry-through structure aft of the cabin, outside the pressure vessel. The increased sweep produces a longer chord length for a given wing thickness, reducing drag. The high sweep angle also improves rotor flapping clearance, allowing shorter pylons and thus minimizing cg shift. Use of the canard permits optimum cg placement.

Figure 3-11 shows a concept for an airliner, also with a canard. As illustrated in the figure, the fuselage can be configured for a load of 75 passengers or a load of typical cargo containers.

Technology issues associated with commercial tilt rotor development include stability and controllability of the canard configuration. This can be evaluated in wind tunnel tests on a typical scale model, as well as performance and loads implications resulting from the impingement of shed vortices from the canards on the rotor discs.

Low wing placement results in a reduced vertical distance from the rotor disc to the vertical cg of the aircraft, reducing control power in the longitudinal (pitch) direction. Analysis shows that small increases in hub flapping restraint will suffice to provide the necessary control moment during hover; however, increased hub stiffness may have an effect on the mechanical stability of the rotor/wing system. Again, this might possibly be investigated in a scale model or perhaps in full scale using the XV-15.

The large stiffness requirement of tilt rotor wings, as well as the cross shafting that must be carried in the wing, results in increased wing thickness. Sweeping the wings produces a greater chord length for a given thickness, but requires careful structural design to prevent instability. Wind tunnel testing of these configurations would be useful and could be done on a scale model.

Tilt-Fold Rotors

The ultimate development of the tilt rotor concept is the tilt-fold configuration. An example of a concept for a tilt-fold fighter is shown in Figure 3-12. The technology to develop this concept in full scale already exists. Bell tested a tilt-fold rotor system sized for the XV-15 in the NASA-Ames 40- by 80-foot

wind tunnel in 1972 (fig. 3-13). Recent developments in convertible engines (fig. 3-14) will make powerplants for this type of aircraft available in the necessary timeframe.

Figure 3-15 shows a possible concept for a shipboard-compatible tilt fold rotor aircraft that could be used for ASW missions among others.

REMOTELY PILOTED VEHICLES (RPVs)

Another interesting advanced configuration study of tilt rotor applications is the field of unmanned aerial vehicles (UAVs) or, as they are more commonly called, RPVs. Conventional fixed-wing RPVs require large, costly equipment for launch and recovery, reducing system mobility and flexibility. Rotary wing concepts permit vertical takeoff and landing, eliminating the launch and recovery systems, but are significantly restricted in cruise performance and efficiency. These same restrictions led to the development of the tilt rotor in the first place.

A recent Navy requirement for a midrange RPV specified high subsonic speeds, a 300-nmi radius of action, air launch capability, and the ability to be landed in the ocean for later recovery by helicopter. Figure 3-16 summarizes these requirements.

Figure 3-17 presents a typical mission profile for the midrange RPV. It will be observed that the purpose of the air launch requirement is to extend the radius of operation. Typically, the RPV would be carried aloft by an A-6 for air launch 100 nmi from the carrier. The RPV would then perform its mission by flying to its target 300 nmi away and returning to its approximate launch point, where it would be dropped in the ocean for recovery by helicopter and then air lifted back to the carrier. The total mission time would be at least 4.25 hours and could go as high as 5.5 hours, if the RPV were as slow as allowed by the specifications.

Figure 3-18 presents a concept for a tilt rotor RPV to perform the mission noted above. Figure 3-19 summarizes the weights and performance of the tilt rotor RPV. Examining this vehicle with regard to Navy requirements shows that the aircraft could take off from any vessel with a 30- by 30-foot pad and, cruising at 204 knots - although somewhat slower than desired - could fly 400 nmi in and 400 nmi back to a vertical landing in only 4 hours, eliminating the requirement for the carrier, the A-6, the helicopter, and the need to flush salt water from the systems upon return (fig. 3-20).

The advantages of a tilt rotor RPV are many. In addition to eliminating the need for launch and recovery equipment (reported to require one C-5A for transport), the aircraft's ability to hover can be used for applications such as soil sampling and operation from unprepared areas. It can be landed and taken off

at the front line by handing off control to a forward operator. This will allow courier service as well as observation. It is much more compatible with shipboard operation since net recovery on a pitching and rolling deck is nearly impossible, while a simple hauldown mechanism will allow landing the tilt rotor from a hover.

Hardware Development

The advantages of the tilt rotor concept in an RPV became obvious, along with a quick, inexpensive way to evaluate it, as engineers were performing wind tunnel model testing for the V-22 program. Figure 3-21 shows a 20-percent Froude scale model of the V-22 undergoing testing in the wind tunnel. The size and direct applicability of some of the model hardware led to an idea for an R&D concept demonstrator. Figure 3-22 shows a sketch of the aircraft. Figure 3-23 presents a schematic of the drive system concept and figure 3-24 shows the nacelle. The control mechanization is similar to that in the XV-15. Figure 3-25 shows the modular concept of the airframe, which will be fabricated from foam core, glass skin sandwich panels.

Figure 3-26 summarizes the weights and performance of a 500-pound gross weight tilt rotor aircraft for use as an RPV. Bell and its tilt rotor partner, Boeing-Vertol, are jointly engaged in the design and fabrication of hardware for the concept demonstrator aircraft. As shown by the schedule in figure 3-27, the first flight is expected in late summer, 1987, with flight demonstrations by the end of the year.

CONCLUSIONS

Part III has presented several future applications of tilt rotor aircraft for both military and commercial markets. These applications offer significant advantages to the user. Indeed, several markets have already been announced and the continued development of the tilt rotor will make it available to fill those needs.

Technology development will allow enhancement of the capabilities of the tilt rotor. Effects of hub stiffness on wing stability, controllability/stability of canard configurations, and effect of high wing sweep on drag are some of the interesting challenges that must be studied prior to full-scale development. The technology exists today to develop a tilt-fold rotor aircraft with speed capabilities in the transonic range.

Finally, hardware development in small-scale models will allow low-cost concept demonstration of a very interesting application of tilt rotor technology.

The future of the tilt rotor is exciting indeed!

MODEL 412 ROTOR SYSTEM WITH COMPOSITE YOKE
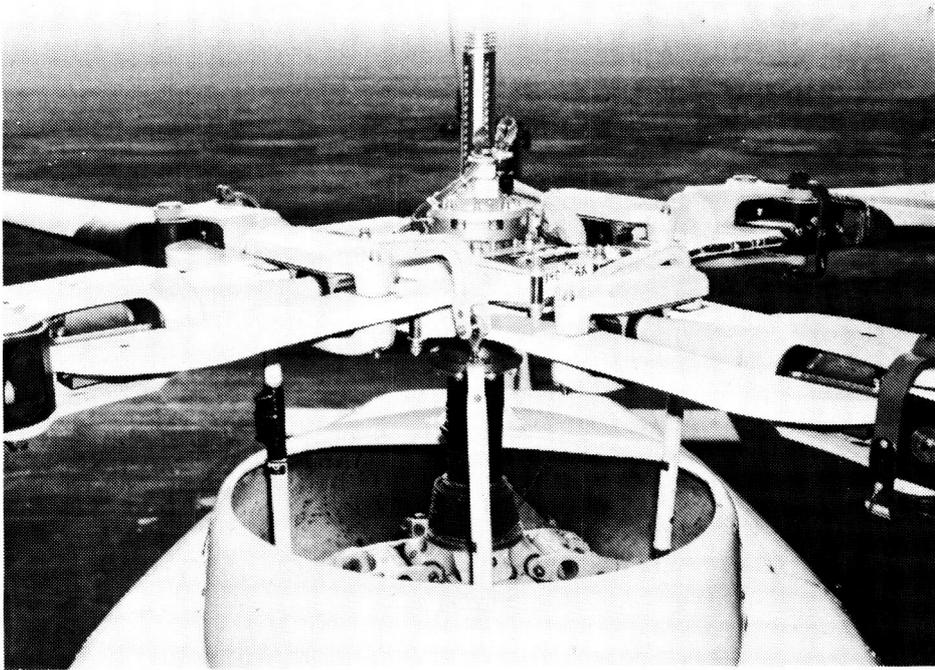
Figure 1-1

OH-58D ROTOR SYSTEM WITH COMPOSITE YOKE

Figure 1-2

MODEL 680 ROTOR SYSTEM

YOKE ASSEMBLY

LEAD-LAG DAMPER

FEATHERING ELEMENT

UPPER CLAMP PLATE

FLAPPING ELEMENT

CUFF ASSEMBLY

SHEAR RESTRAINT

LEAD-LAG DAMPER
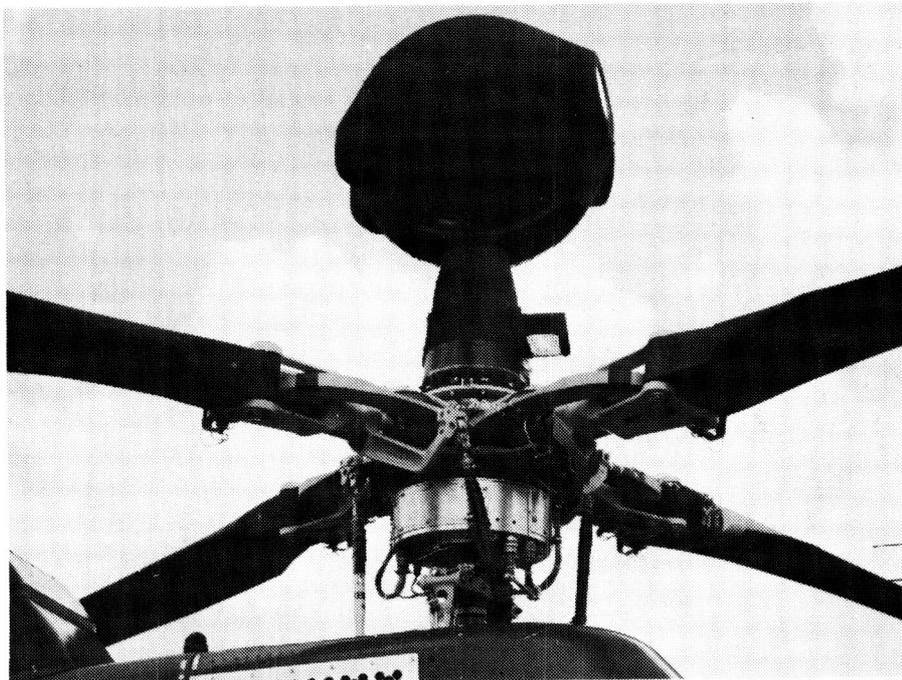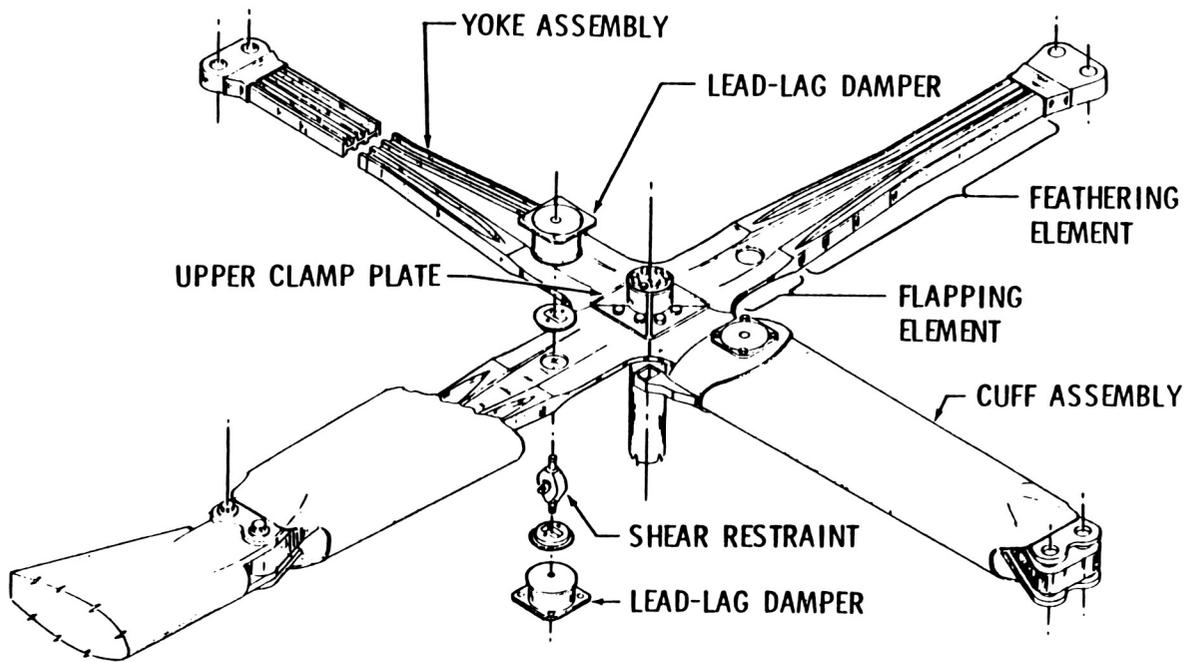
Figure 1-3

FIBERGLASS/EPOXY FILAMENT WOUND BELT FOR MODEL 680 YOKE ASSEMBLY
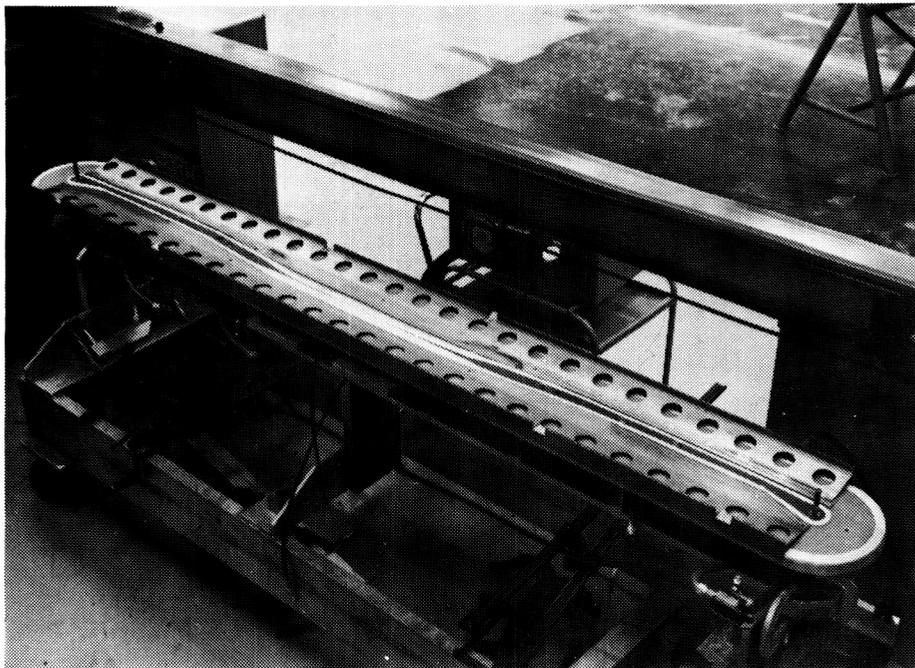
Figure 1-4

MODEL 680 CAVITY BOND TOOL
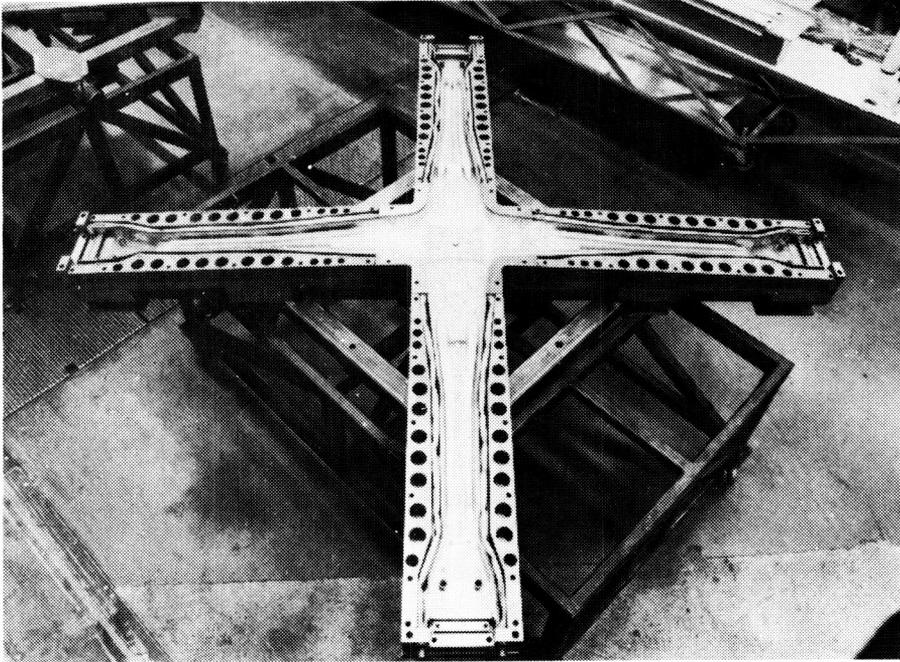
Figure 1-5

LAYERED FINITE ELEMENT
MODEL OF QUARTER YOKE
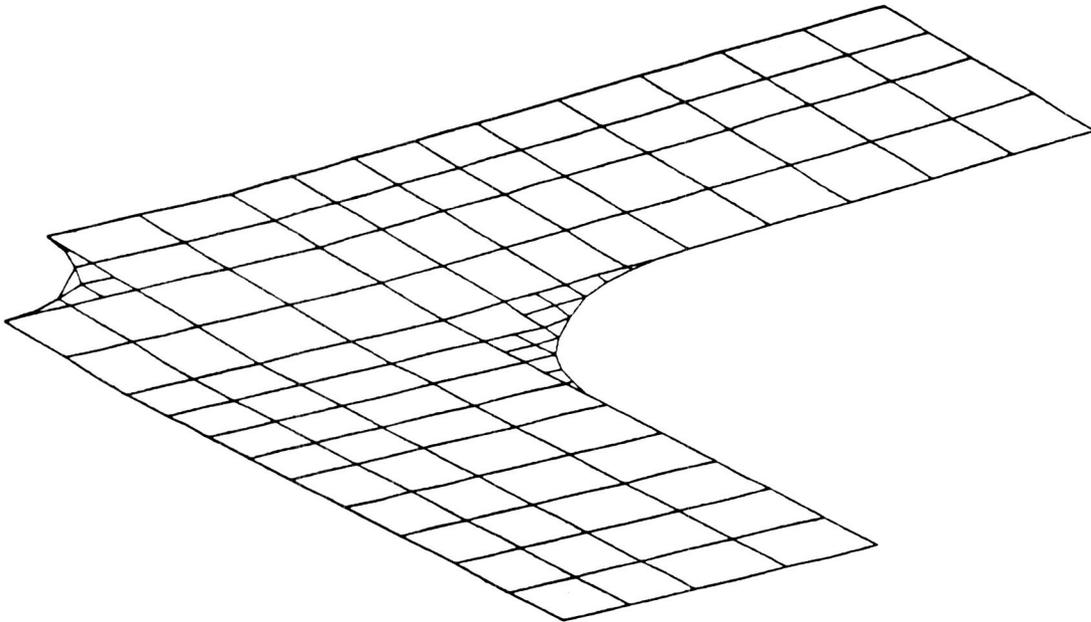
Figure 1-6

TWO-DIMENSIONAL FINITE ELEMENT
MODEL OF SPANWISE SECTION OF YOKE
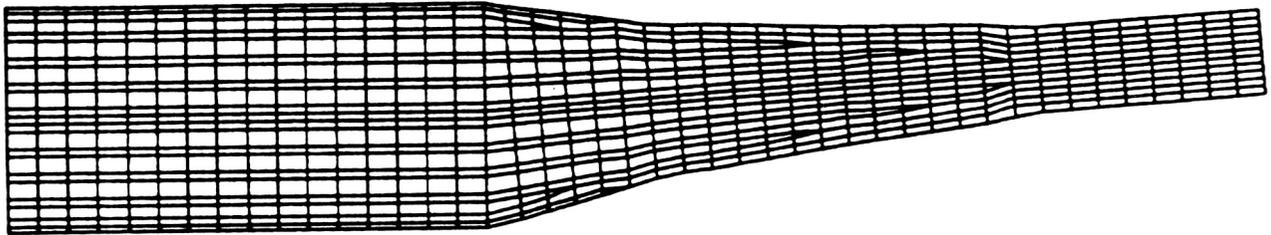
Figure 1-7

CENTER SECTION OF SECOND
GENERATION MODEL 680 YOKE
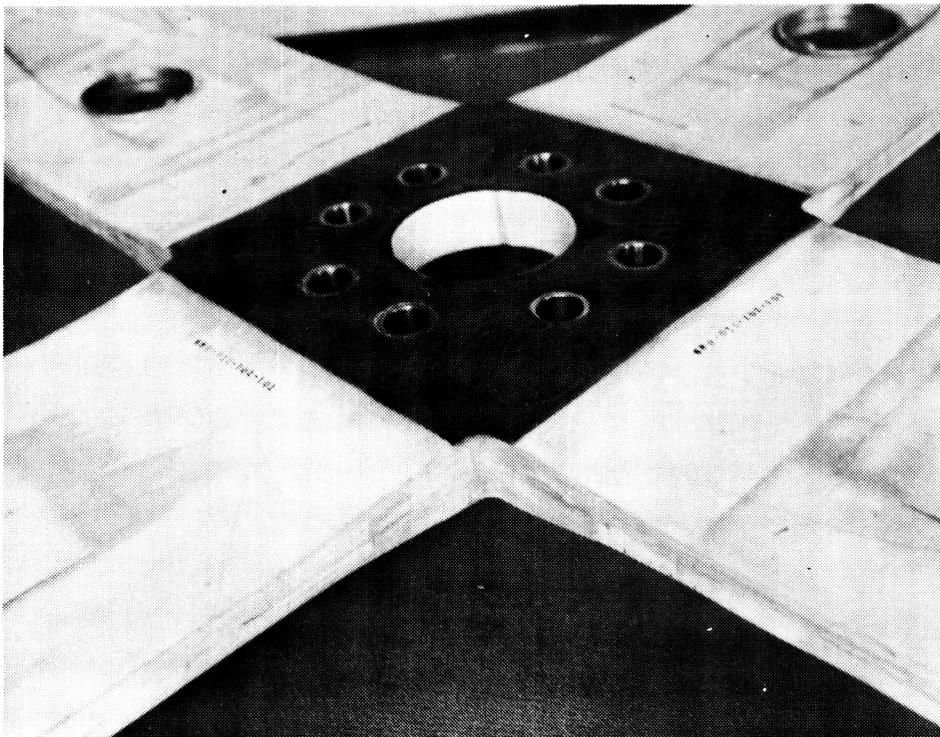
Figure 1-8

ADHESIVE INNER LAYER FOR
DELAMINATION ARRESTMENT

BASIC CONCEPT
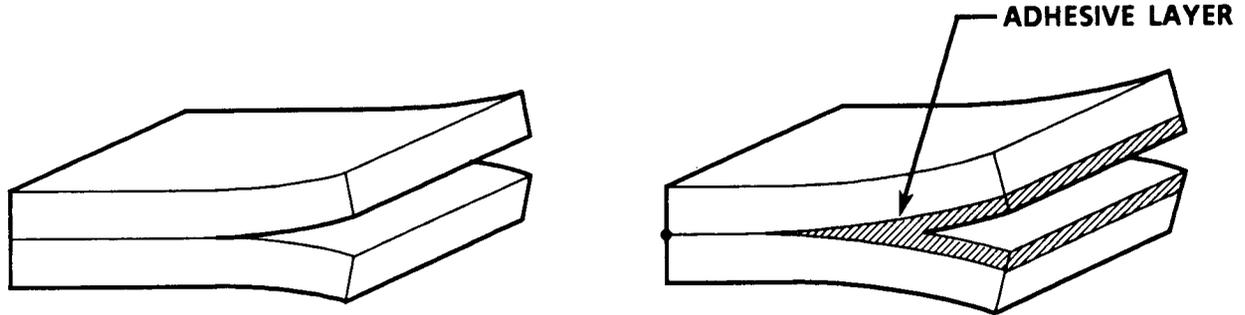
BRITTLE FRACTURE

DUCTILE FRACTURE

Figure 1-9

INTERLAMINAR NORMAL STRESS
DISTRIBUTION THROUGH THE THICKNESS
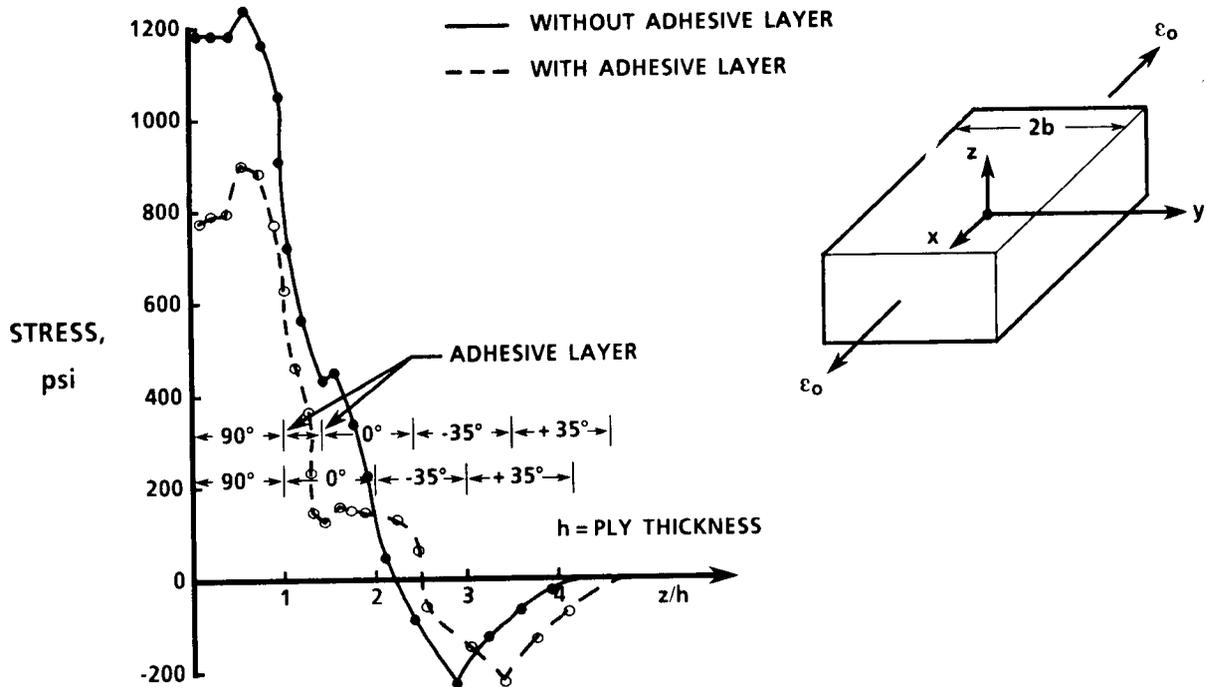
Figure 1-10

X-RAY RADIOGRAPHY OF TEST COUPONS
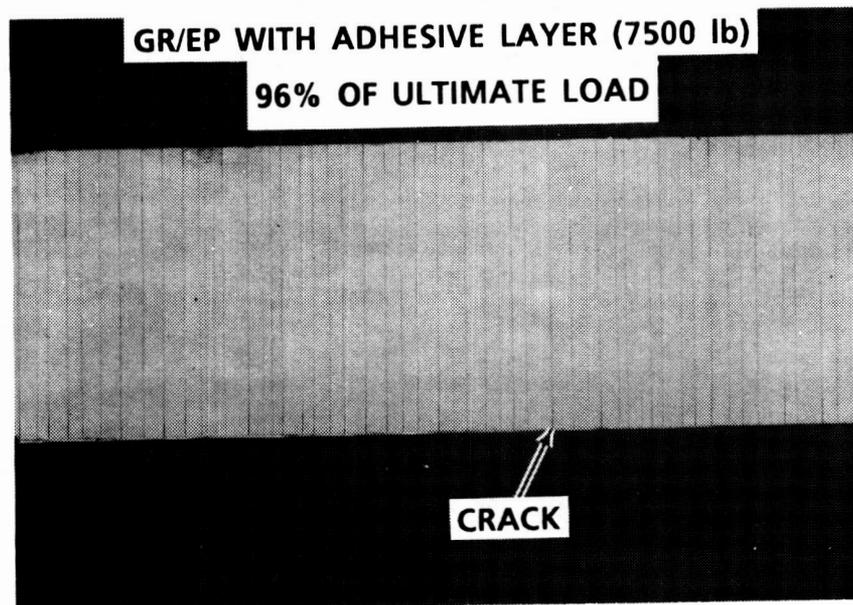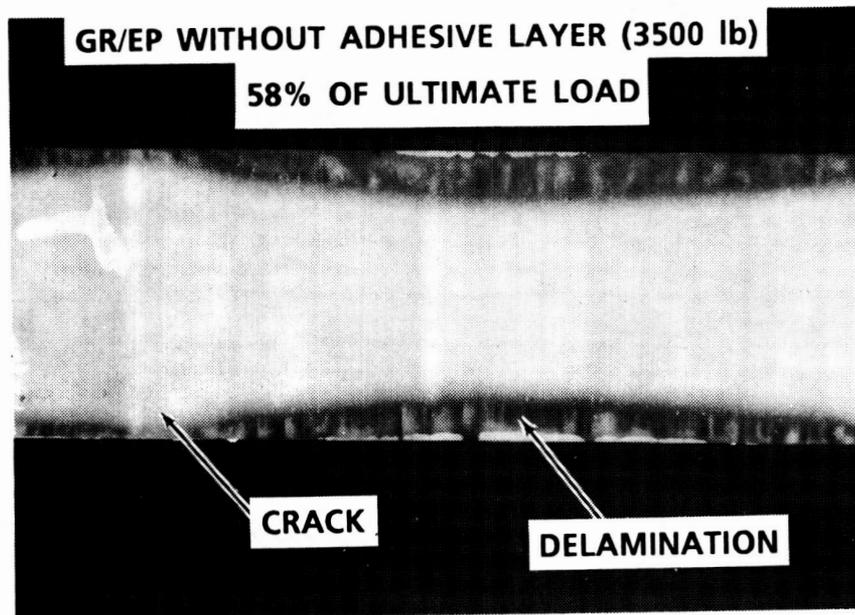
Figure 1-11

PHOTOMICROGRAPH OF TEST
COUPON WITH TRANSVERSE CRACK

GR/EP WITH ADHESIVE LAYER (FINAL FAILURE)

90° PLY CRACK

ADHESIVE INNER LAYER

Figure 1-12

MODEL 680 ROTOR SYSTEM IN FLIGHT

Figure 1-13

MODEL 680 VIBRATION SUMMARY

222/680 LOAD LEVEL SURVEY AUGUST 1982
ALL SEATS, ALL DIRECTIONS, ALL G.W./C.G.'s
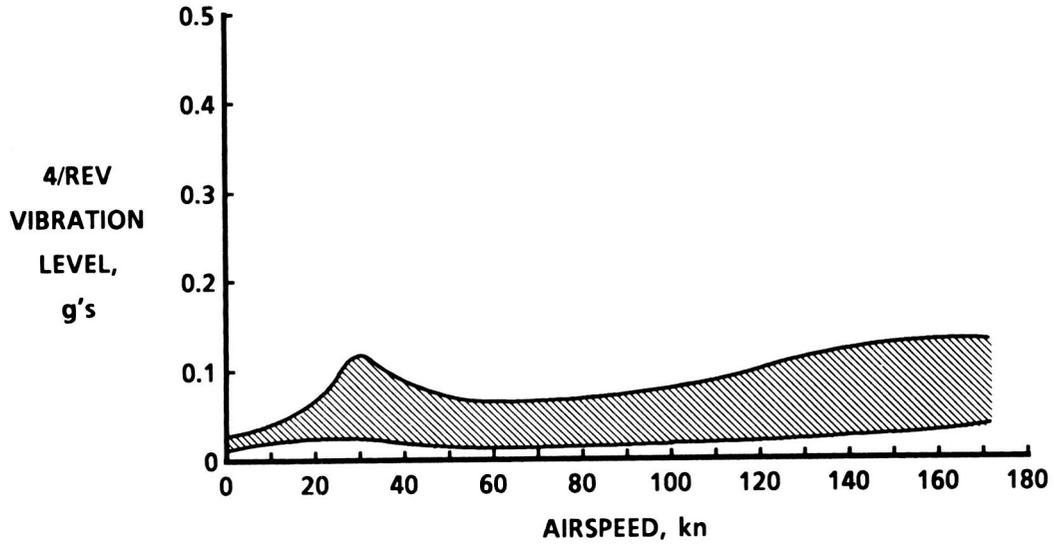
Figure 1-14

ALR BLADE TOOLING
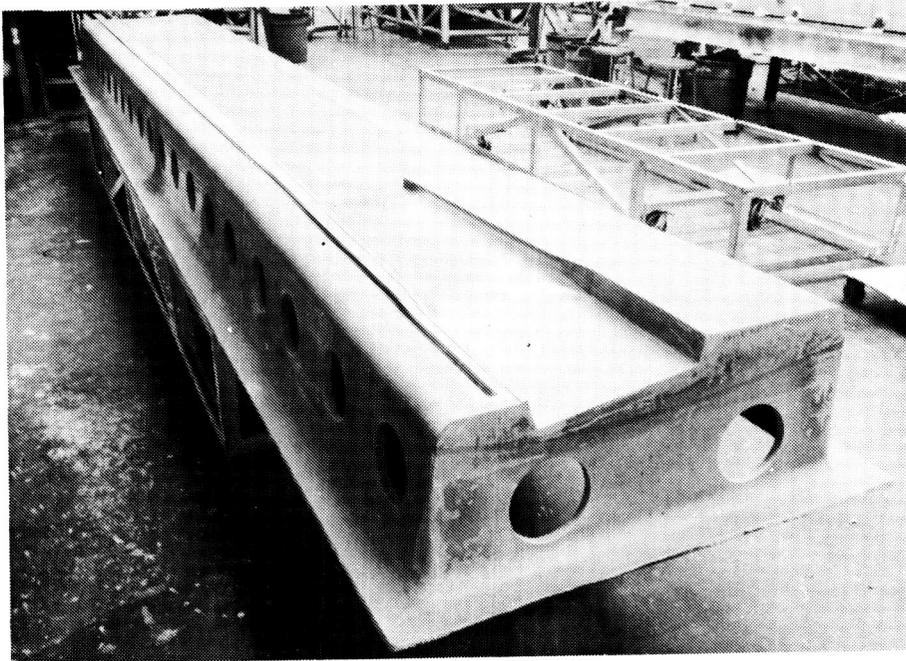
Figure 1-15

ALR BLADES WITH MODEL 680 ROTOR HUB
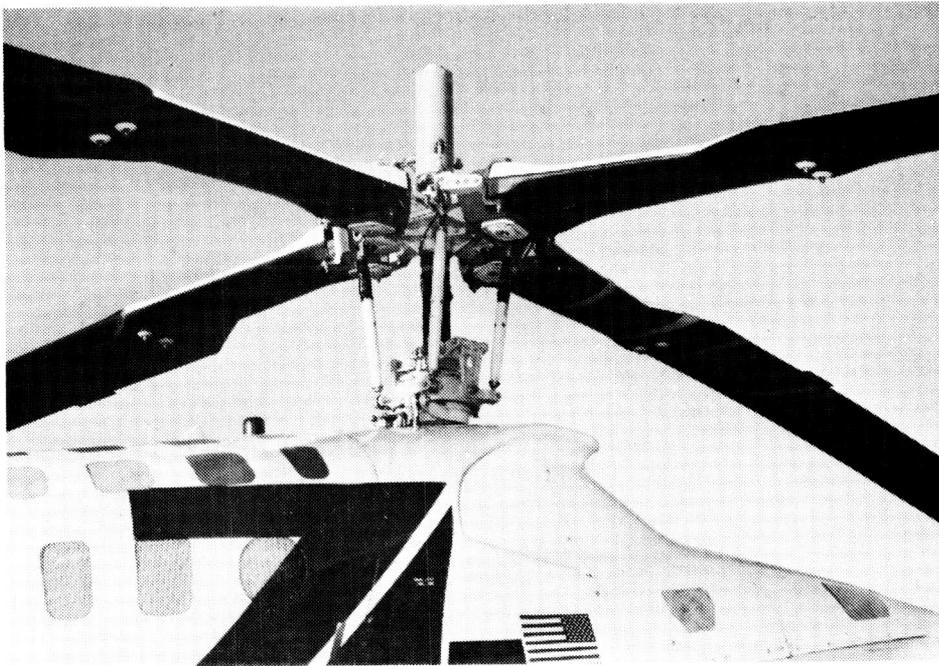
Figure 1-16

BELL ADVANCED BEARINGLESS ROTOR SYSTEM FOR 14,000 - 18,000 POUND HELICOPTERS
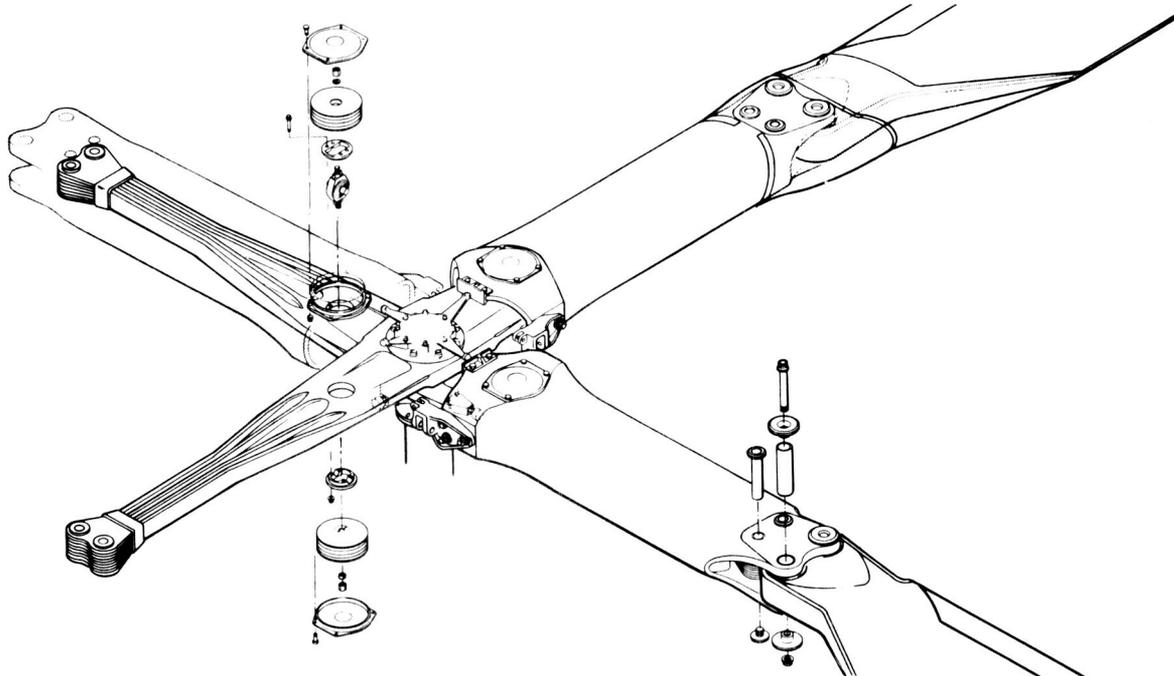
Figure 1-17

AH-1W HELICOPTER WITH ADVANCED BEARINGLESS ROTOR SYSTEM
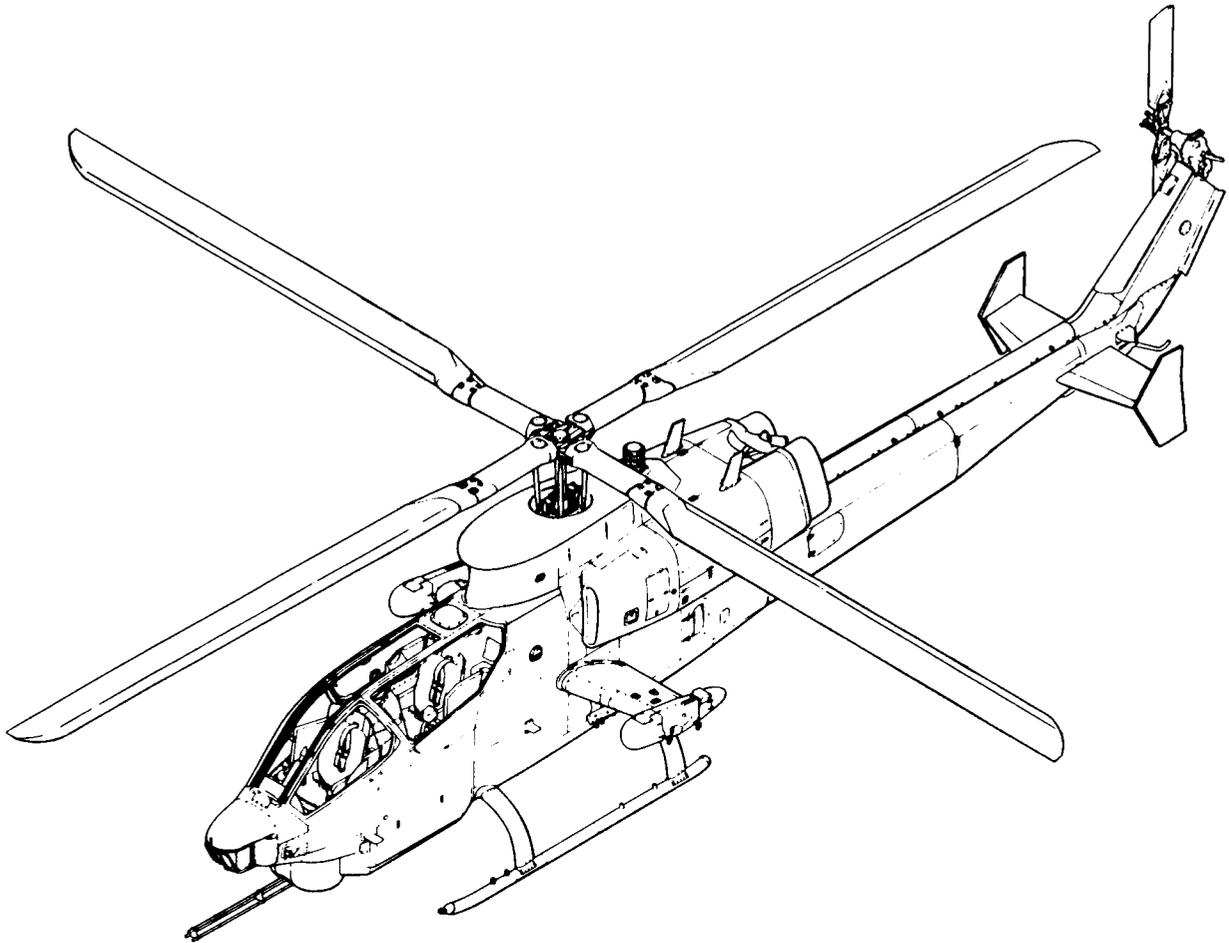
Figure 1-18

COMPARISON OF BHTI ROTOR AIRFOIL CHARACTERISTICS
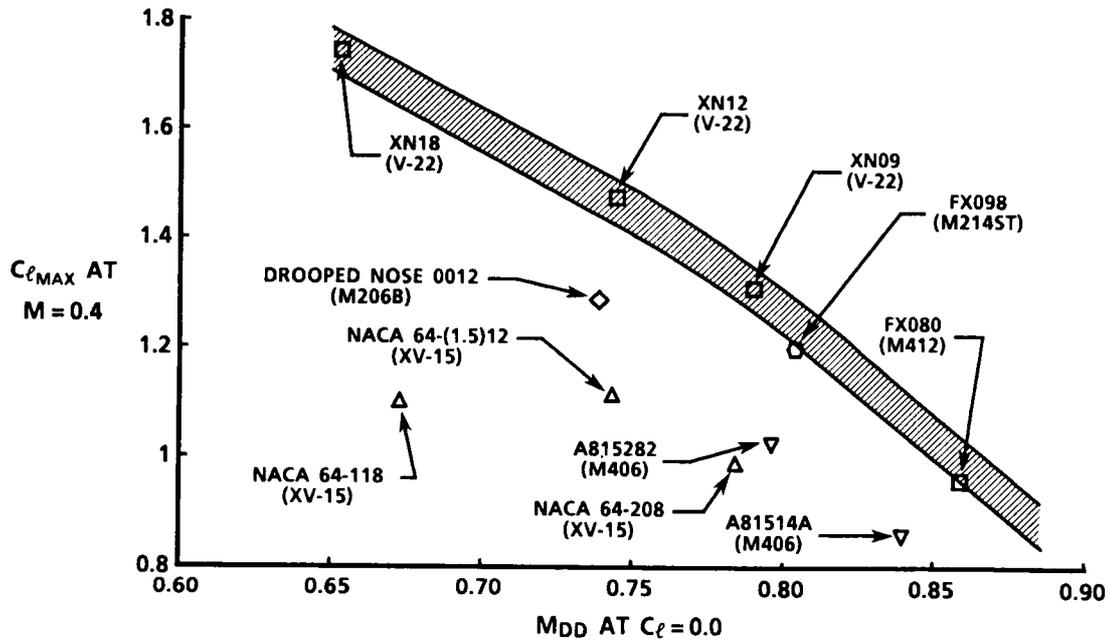
Figure 2-1

TILT ROTOR AIRFOIL DESIGN GOALS AND CONSTRAINTS

RADIAL STATION r/R	DESIGN CONSTRAINTS		AERODYNAMIC DESIGN OPTIMIZATION GOALS			
	t/C	INCOMP. C_{m_0}	MANEUVER ($C_{\ell max}$)	CRUISE (C_d)	MAX. SPEED (M_{DD})	HOVER (L/D_{max})
1.0	0.09	-0.02	1.35 @ M = 0.6	0.006 @ C_ℓ = 0.3 M = 0.75	0.81 @ C_ℓ = 0.3	80.0 @ M = 0.65
0.75	0.12	-0.03	1.40 @ M = 0.45	0.006 @ C_ℓ = 0.2 M = 0.65	0.72 @ C_ℓ = 0.2	95.0 @ M = 0.5
0.50	0.18	-0.05	1.50 @ M = 0.3	0.007 @ C_ℓ = 0.0 M = 0.57	0.64 @ C_ℓ = 0.0	80.0 @ M = 0.3
0.25	0.28	-0.12	1.35 @ M = 0.19	0.018 @ C_ℓ = 0.0 M = 0.51	0.59 @ C_ℓ = 0.0	50.0 @ M = 0.2

Figure 2-2

COMPARISONS OF DESIGN GOAL WITH WIND TUNNEL DATA, XN-12 AIRFOIL
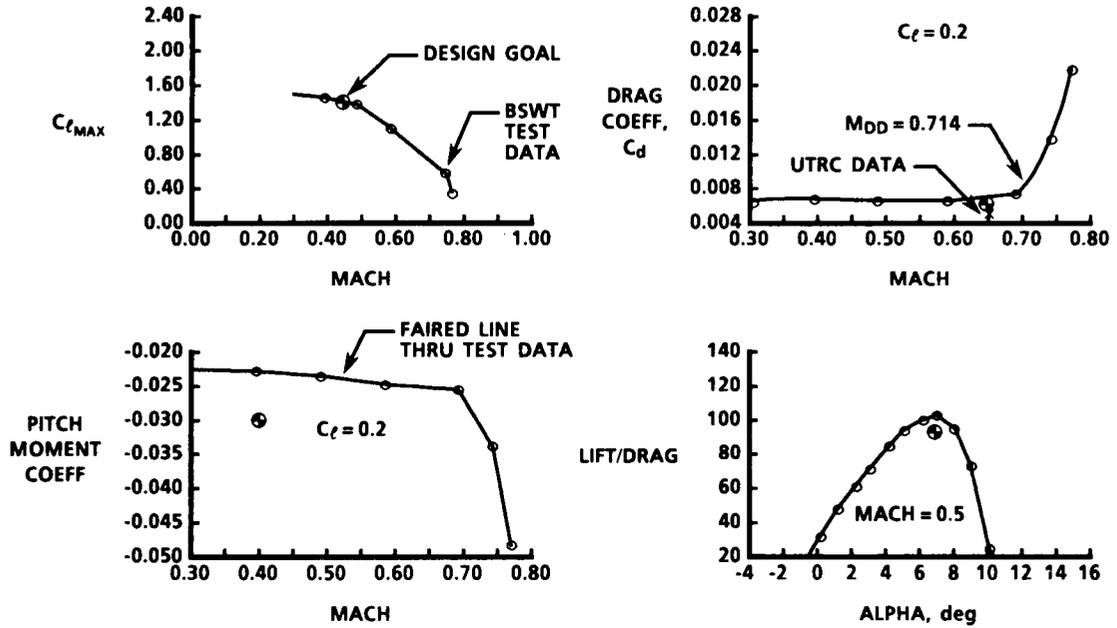
Figure 2-3

ROT22/OLS PRESSURE DISTRIBUTION CORRELATION AT 95 PERCENT RADIUS
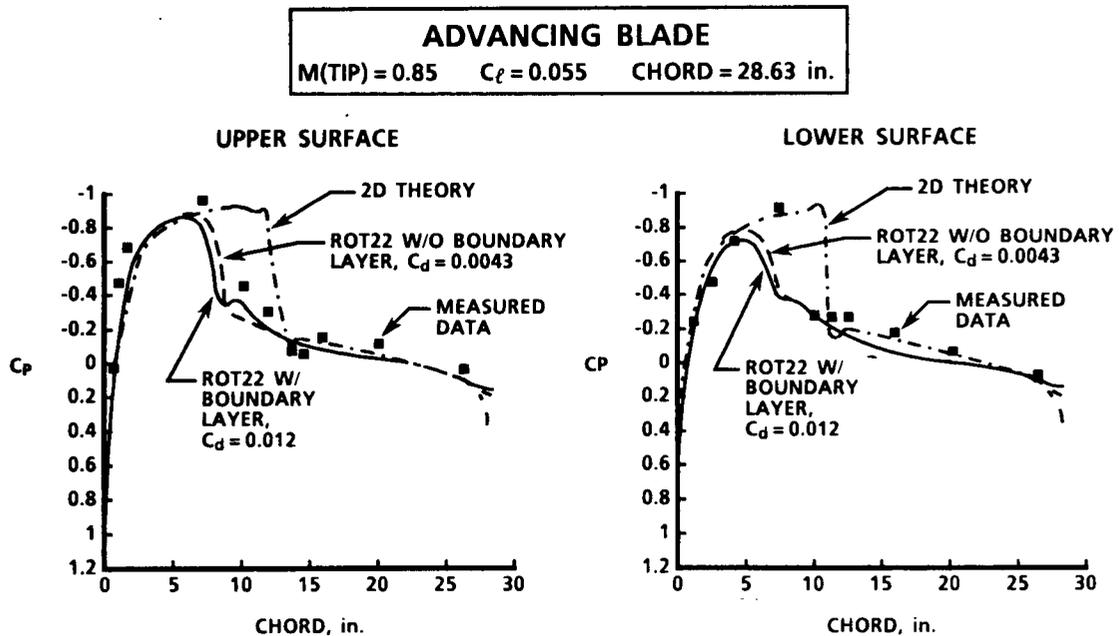
Figure 2-4

C81 NONUNIFORM INFLOW CORRECTION FACTOR
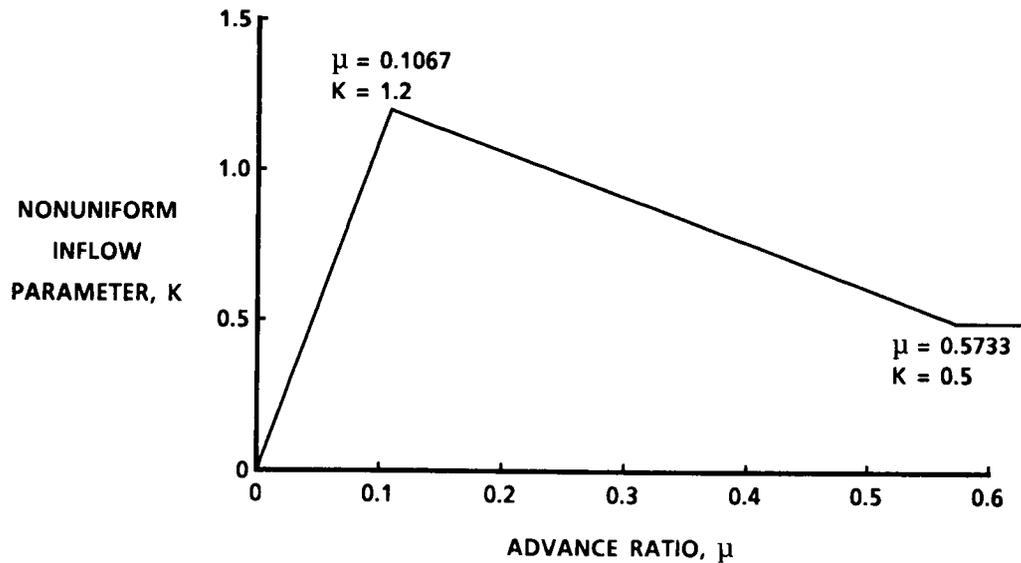
Figure 2-5

CORRELATION IN LATERAL FLAPPING

$C_{T/\sigma}$ = 0.08	TIP SPEED = 450 ft/sec	SOLIDITY = 0.0892
α_{TPP} = +1°	RADIUS = 2.73 ft	CORE = 0.05
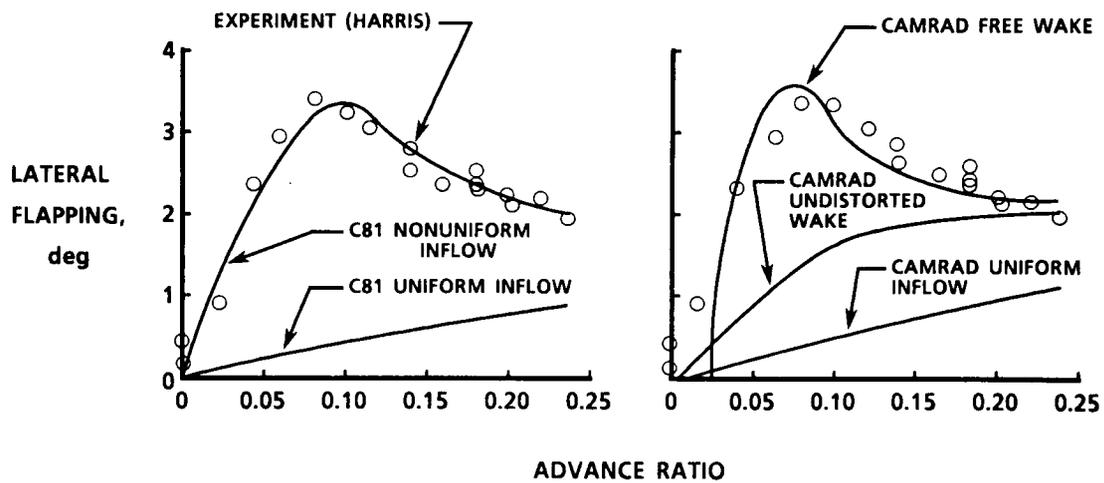
Figure 2-6

CORRELATION IN LONGITUDINAL FLAPPING

$C_{T/\sigma}$ = 0.08	TIP SPEED = 450 ft/sec	SOLIDITY = 0.0892
α_{TPP} = +1°	RADIUS = 2.73 ft	CORE = 0.05
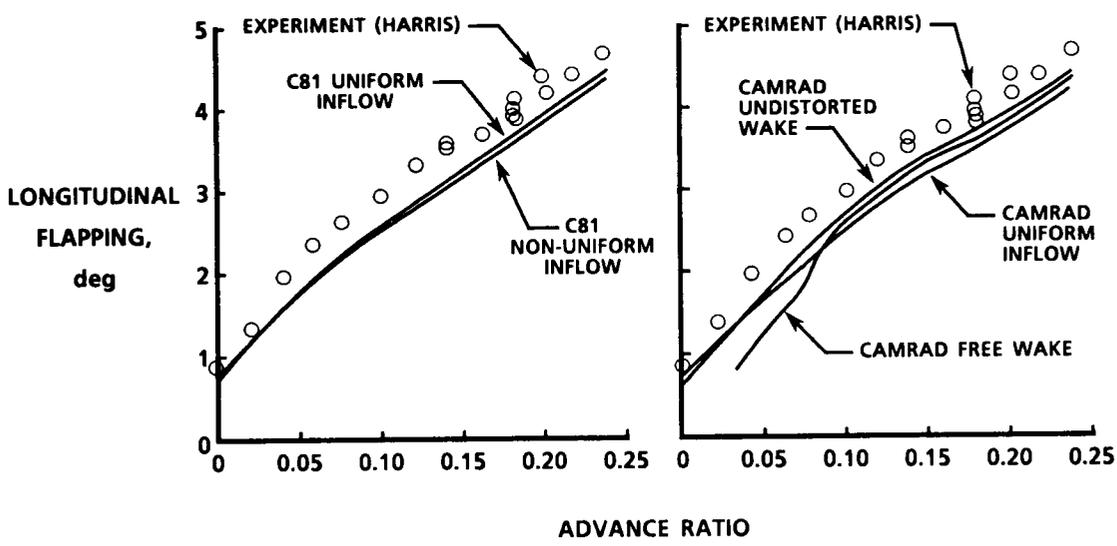
Figure 2-7

CORRELATION IN ROTOR POWER

$C_{T/\sigma}$ = 0.08	TIP SPEED = 450 ft/sec	SOLIDITY = 0.0892
α_{TPP} = +1°	RADIUS = 2.73 ft	ΔC_d = 0.006
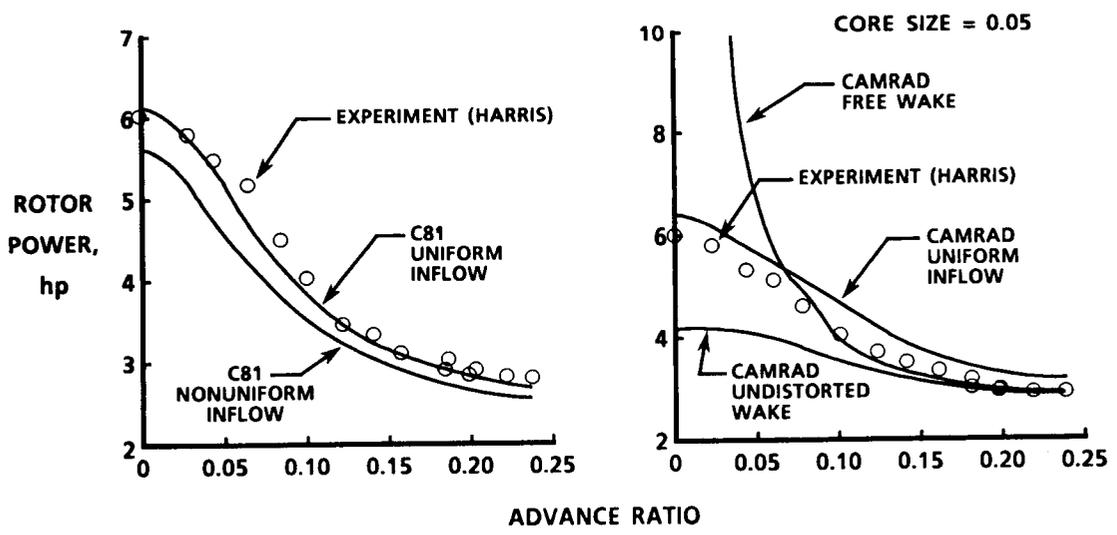
Figure 2-8

FORE AND AFT INDUCED-VELOCITY DISTRIBUTIONS

$C_{T/\sigma}$ = 0.08	TIP SPEED = 450 ft/sec	SOLIDITY = 0.0892
α_{TPP} = +1°	RADIUS = 2.73 ft	ADVANCE RATIO = 0.08

INDUCED VELOCITY/ TIP SPEED

C81 NONUNIFORM INFLOW

CORE SIZE = 0.05

CAMRAD FREE WAKE

CAMRAD UNDISTORTED WAKE

BLADE RADIUS - VIEWED FROM THE LEFT
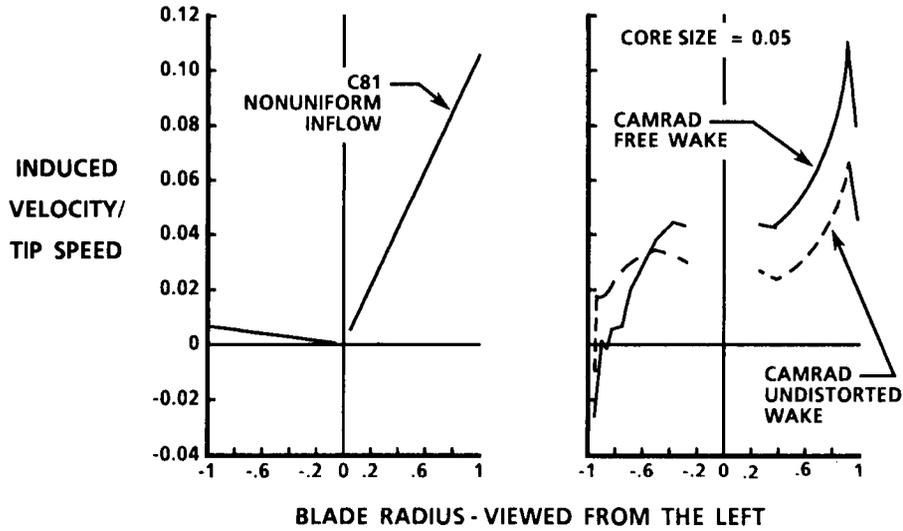
Figure 2-9

XV-15 HOVER PERFORMANCE CORRELATION

ISOLATED ROTOR

ROTOR POWER COEFFICIENT, X 10⁴

• OARF TEST 910, RUN 15
− AR7906

OPERATING GW 13,000 lb

ROTOR THRUST COEFFICIENT, X 10³
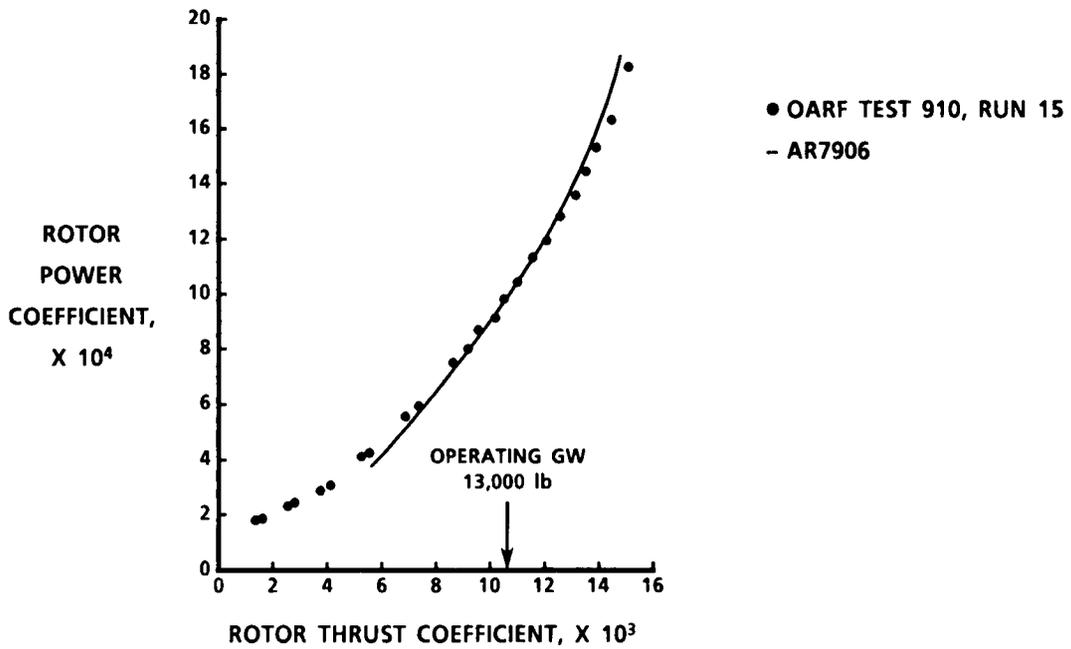
Figure 2-10

XV-15 PROPROTOR EFFICIENCIES CORRELATION

ISOLATED ROTOR

PROPELLER
ADVANCE
RATIO

J = 1.06

J = 1.64

J = 2.12

● 40 x 80 TEST

– AR7907

PROPELLER
EFFICIENCY,
η

PROPELLER POWER COEFFICIENT, C_P
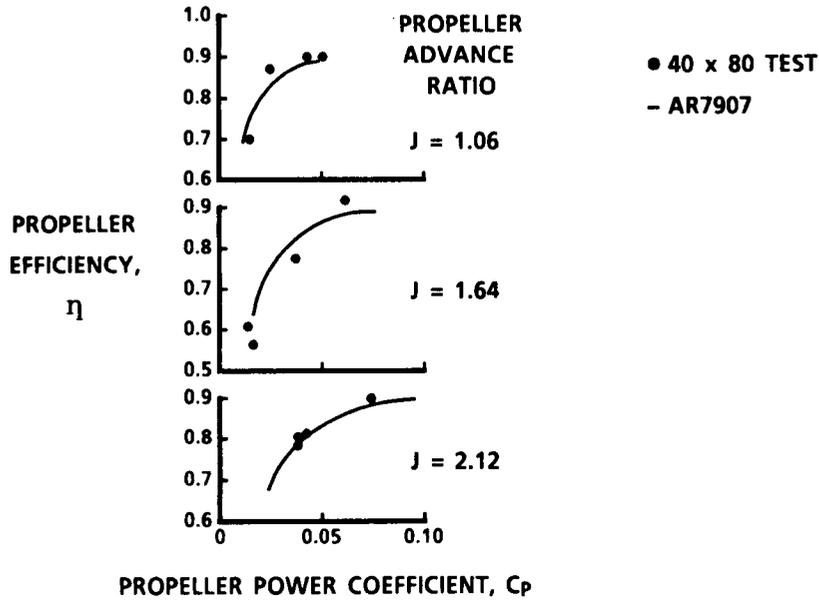
Figure 2-11

CONVERSION MODE XV-15 PROPROTOR PERFORMANCE CORRELATION WITH THEORY

ISOLATED ROTOR

40 X 80 TEST DATA PT.	O	□	◇	△	▽	▷
NACELLE ANGLE	77°	77°	60°	60°	30°	30°
ADVANCE RATIO	0.18	0.32	0.23	0.32	0.24	0.34

ARAM45

ARAM45

THRUST
COEFFICIENT,
C_T

ROTOR POWER COEFFICIENT, C_P

PROPULSIVE FORCE COEFFICIENT, C_X
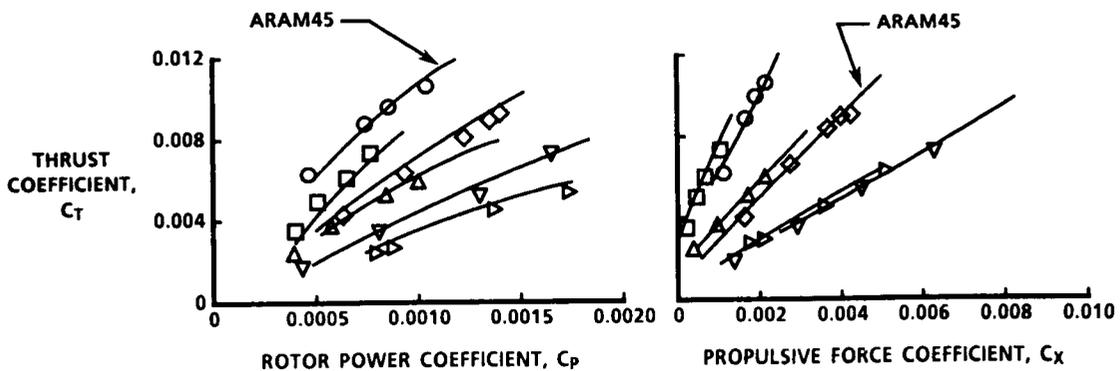
Figure 2-12

VSAERO AND TEST CORRELATION
ASPECT RATIO 30 WING PANEL MODEL

WSU 85: RUN 91 TEST DATA
TWO-DIMENSIONAL V-22 WING SECTION
$\alpha_{WING} = 5°$ $\delta_{FLAP} = 30°$ MACH = 0.2   Re = 2.0 X 10^6

o   TEST RESULTS
—   VSAERO RESULTS
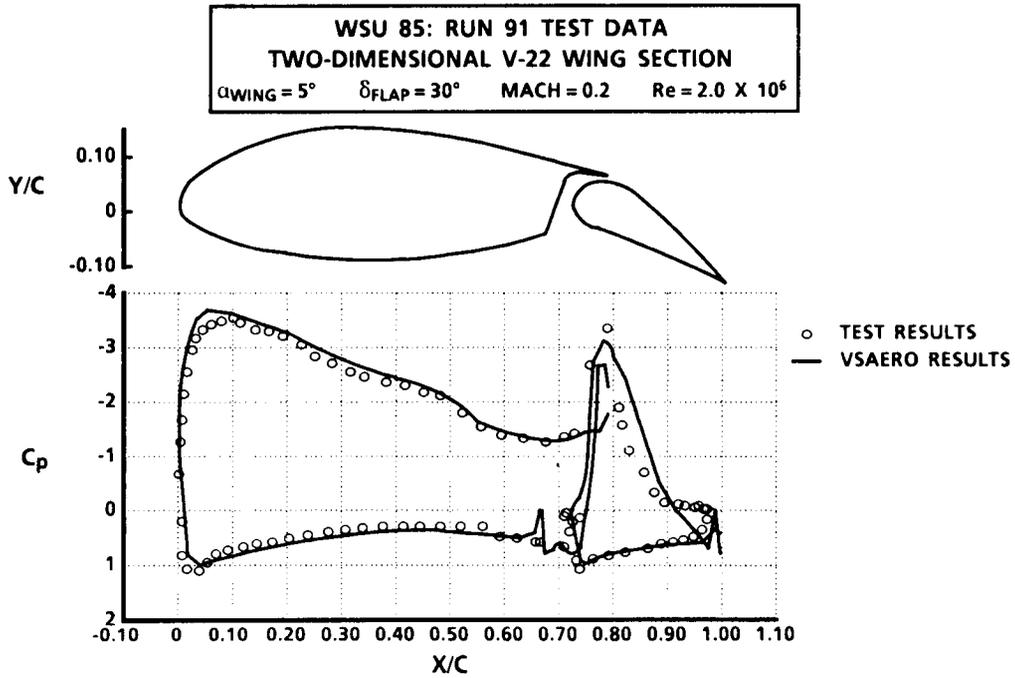
Figure 2-13

VSAERO AND TEST CORRELATION
V-22 SPINNER PANEL MODEL

LSWT 693: RUN 15 TEST DATA
PRESSURE DATA RESULTS CLEAN SPINNER
$\psi_{SPINNER} = 14°$ MACH = 0.226   Re = 1.59 X 10^6

–   VSAERO RESULTS
●   TEST DATA

NACELLE STATION, in.

Figure 2-14

1318
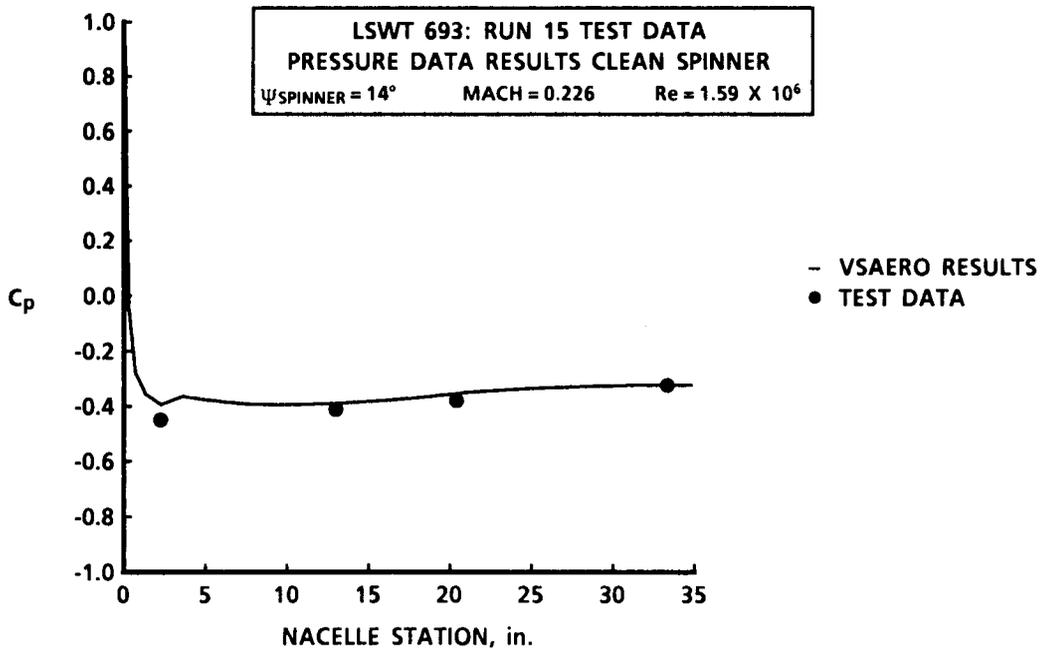
VSAERO AND TEST CORRELATION
WING/NACELLE PANEL MODEL

BVWT 306: RUN 48 TEST DATA

V-22 NACELLE STATION = 359.9 α_{WING} = 20°   INCIDENCE$_{NACL}$ = 0.0°   MACH = 0.2

⊙ TEST RESULTS
- - - VSAERO RESULTS
—— SHAPE

$C_P = 1$

WL, in.

BL, in.
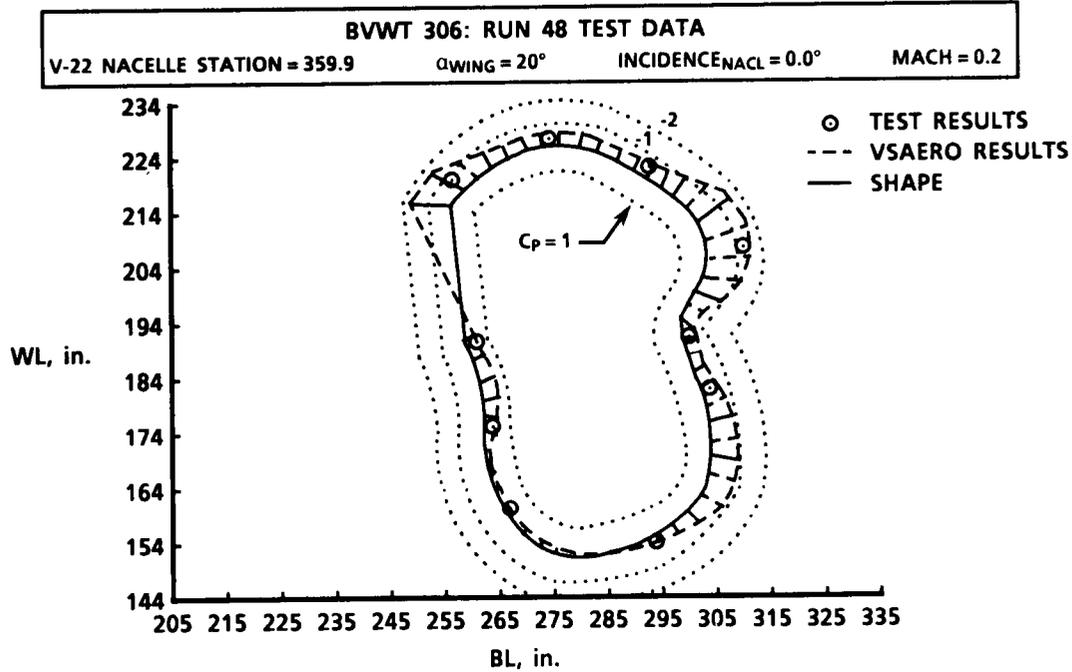
Figure 2-15

VSAERO AND TEST CORRELATION
V-22 INLET PANEL MODEL

BVWT 306: RUN 221.5 TEST DATA
V-22 0.4 SCALE NACELLE/INLET MODEL
α_{WING} = 0°   INCIDENCE$_{NACL}$ = 90°   MAX POWER HOVER

RADIAL POSITION

PRESSURE PORT LOCATIONS

STATIC PRESSURE / TOTAL PRESSURE

TEST DATA (SYMBOLS)

VSAERO RESULTS (LINES)

FUSELAGE STATION, in.

Figure 2-16

1319
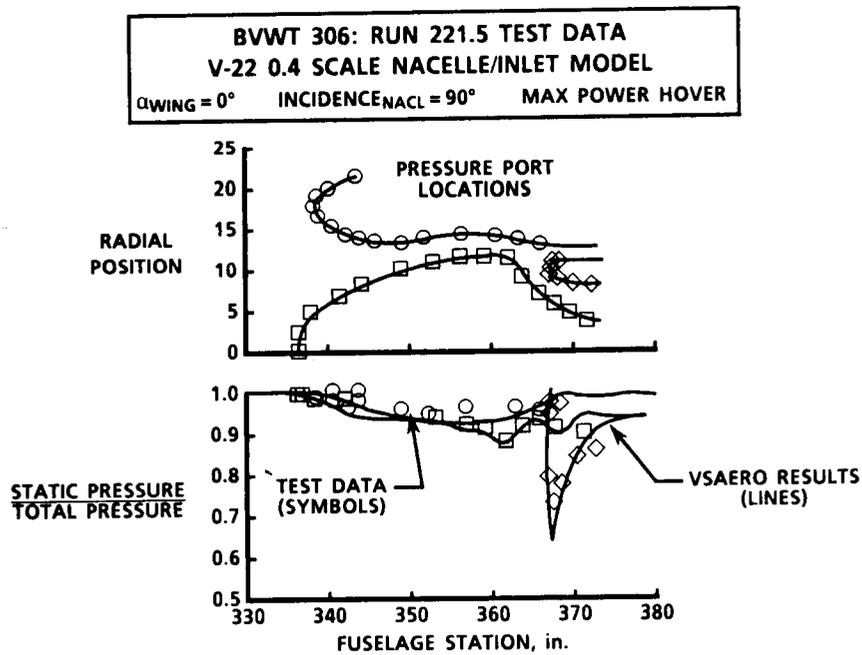
VSAERO TILT ROTOR AIRLOAD DISTRIBUTION
EMPENNAGE PANEL MODEL
SYMMETRICAL PULLOUT

$\alpha_{EMP} = 7°$	$\delta_{ELEVATOR} = 0°$	$\delta_{RUDDER} = 0°$

BEAM BENDING MOMENT, in.-lb x 10³

BUTT LINE, in.
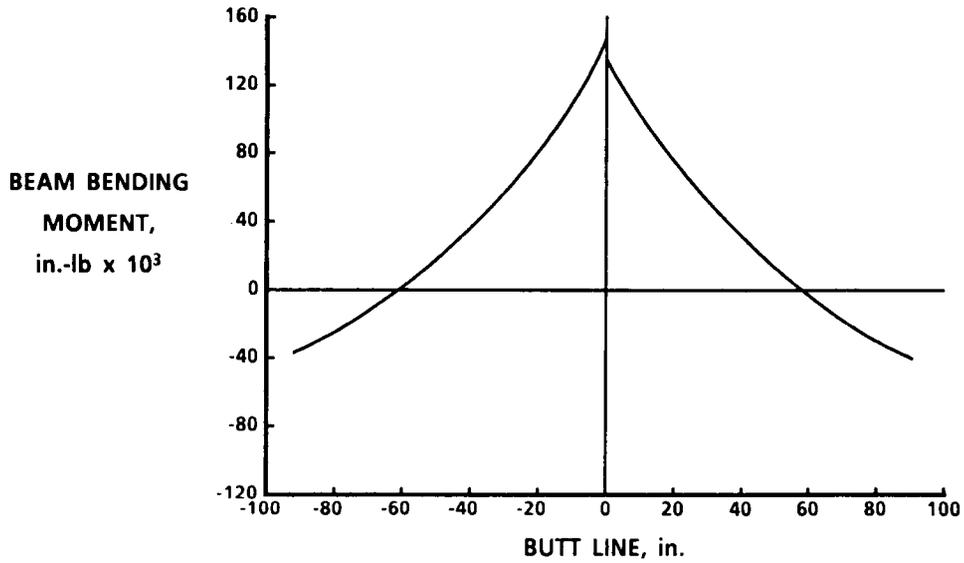
Figure 2-17

NORMALIZED 4/REV VERT. HUB SHEAR & 3/REV BLADE ROOT BEAM MOMENT VS AIRSPEED

4/REV HUB SHEAR

3/REV BLADE ROOT MOMENT

AIRSPEED, KTAS

TYPE ROTOR	THEORY	1982 W.T. DATA
CONVENTIONAL	——	o
NODALIZED	— — —	△
AERODYNAMICALLY OPTIMIZED NODALIZED	□	
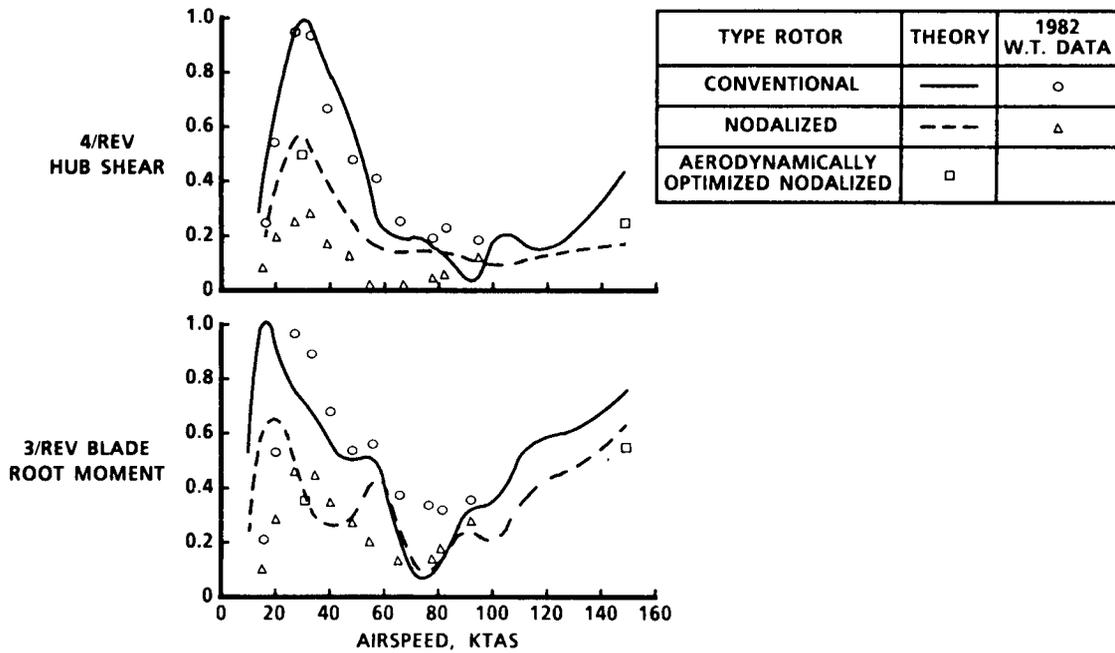
Figure 2-18

TYPICAL GEOMETRY FOR TILT ROTOR AIRCRAFT IN AIRPLANE MODE

AND THE INTERFERENCE VELOCITIES, ΔU_p & ΔU_t
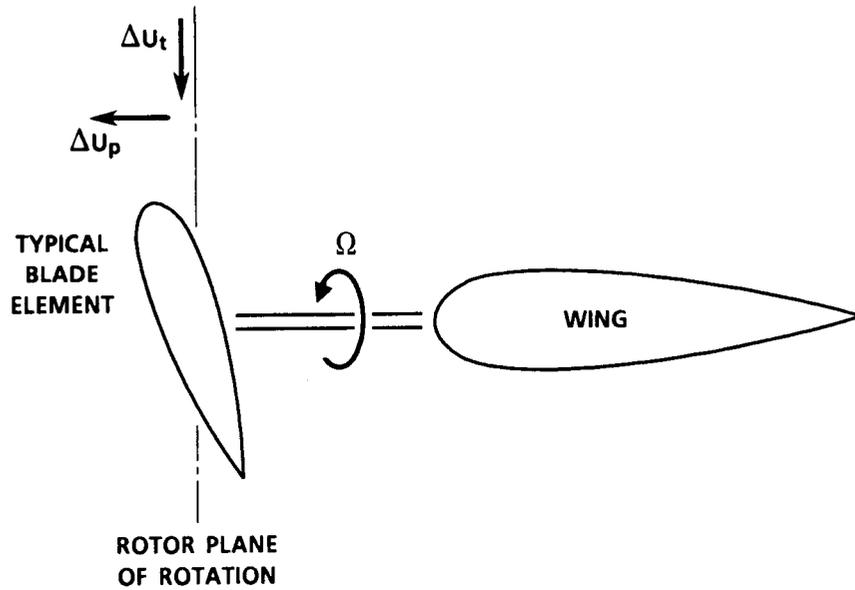
Figure 2-19

DYN5 SIMPLIFIED ANALYTICAL MODEL OF THE WING'S FLOW FIELD

FLOW PROBLEM

MATH MODEL
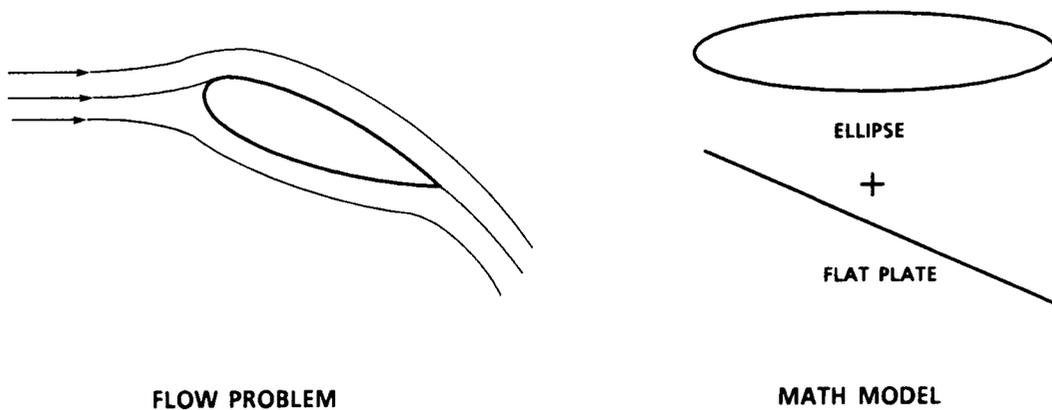
Figure 2-20

CHANGE IN FLOW FIELD AT BLADE 60% RADIUS DUE TO THE PRESENCE OF AIRFRAME

AIRPLANE MODE, 313 KNOTS

—— VSAERO

- - - DYN5
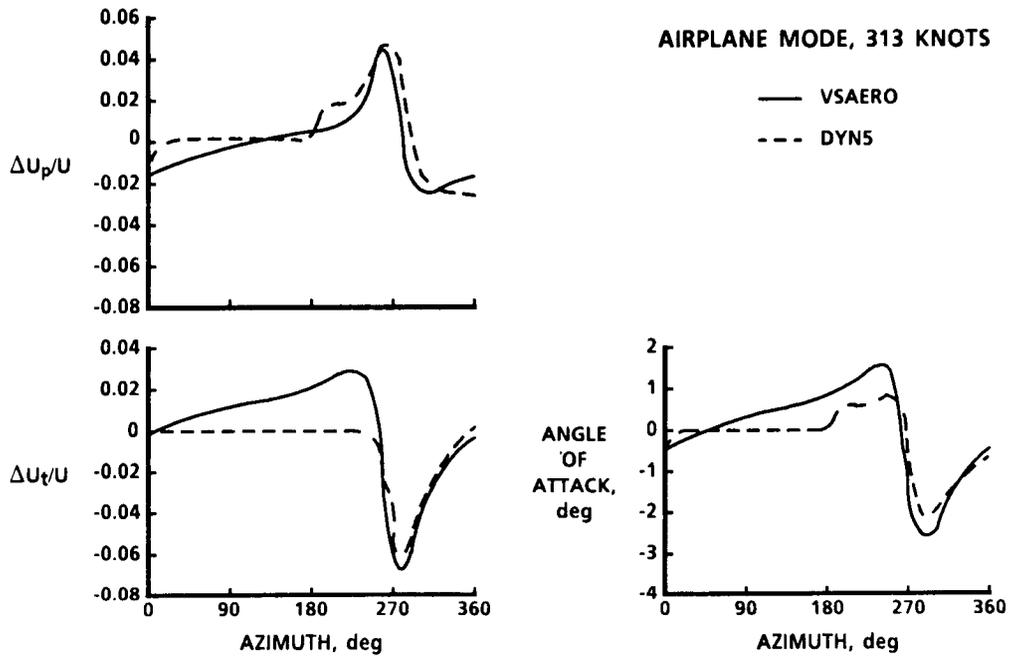
Figure 2-21

COMPARISON OF MEASURED AND CALCULATED BEAMWISE MOMENTS

V = 100 KEAS, RPM = 742, AIRPLANE MODE, WINDMILL

O V-22, 0.2 SCALE, 3RD ENTRY, SEMI SPAN, RUN 152
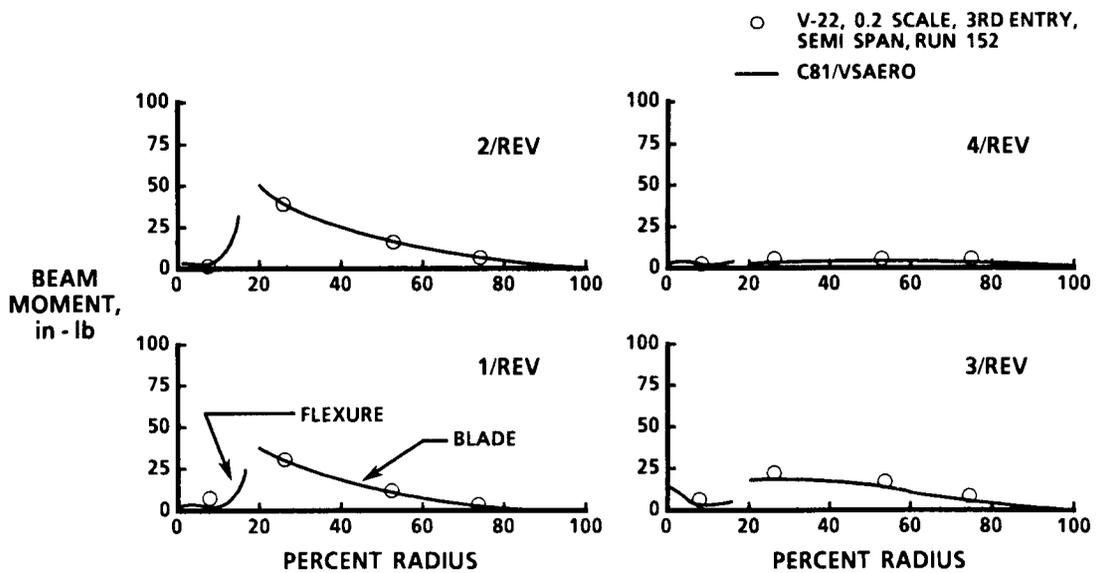
—— C81/VSAERO

Figure 2-22

COMPARISON OF MEASURED AND CALCULATED CHORDWISE MOMENTS

V = 100 KEAS, RPM = 742, AIRPLANE MODE, WINDMILL

○   V-22, 0.2 SCALE, 3RD ENTRY,
    SEMI SPAN, RUN 152
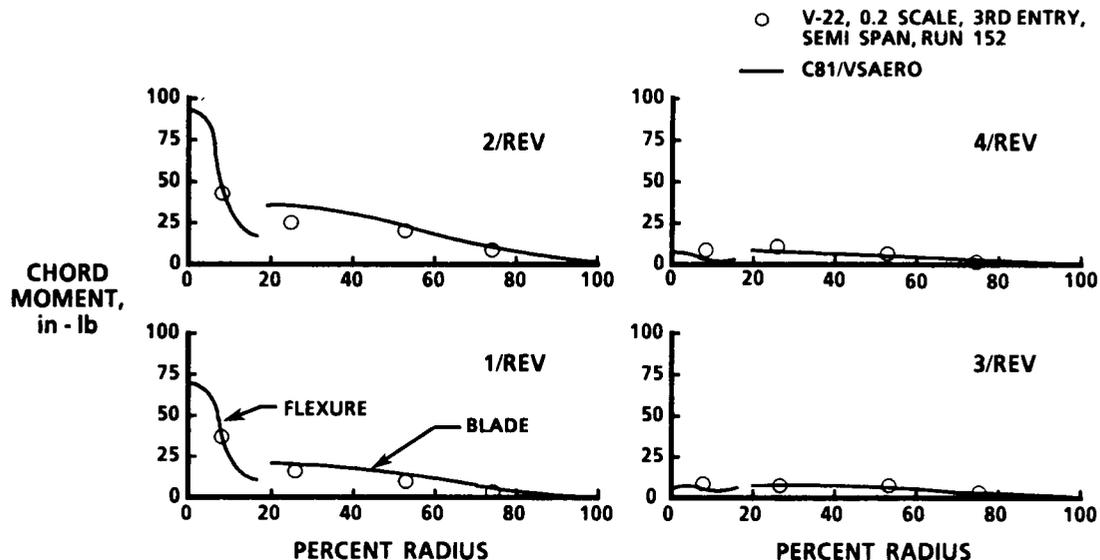
—— C81/VSAERO

Figure 2-23

V-22 0.2-SCALE HUB SHEARS CALCULATED USING C81/VSAERO
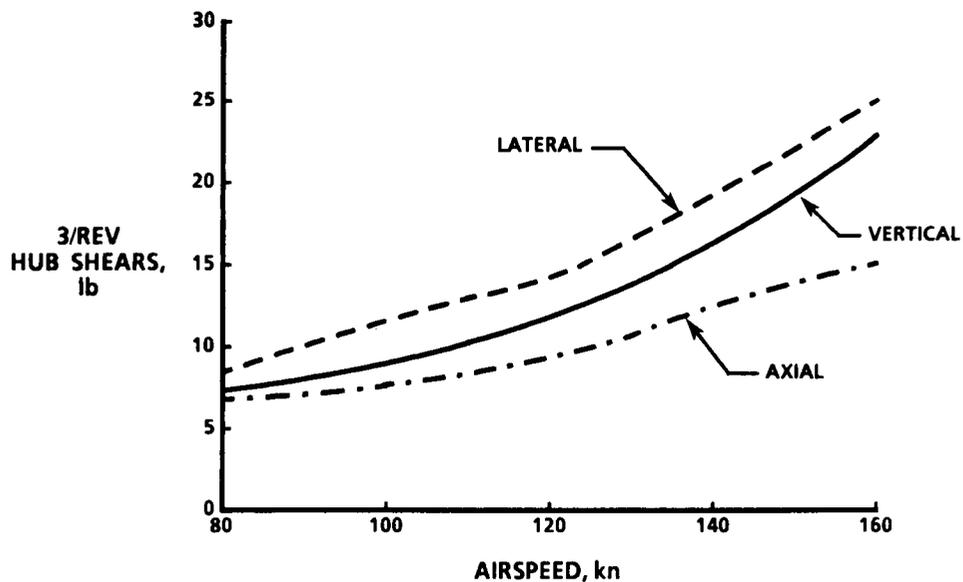
Figure 2-24

WINGTIP BOX FREQUENCY SUMMARY
PYLON AT 90° (HELICOPTER MODE)

MODE DESCRIPTION	MEASURED FREQUENCY (Hz)	ANALYSIS FREQUENCY (Hz)	
		PRETEST	POSTTEST
FIRST WING BEAMWISE BENDING	4.570	4.863	4.664
PYLON PITCH	5.202	4.514	4.89
PYLON YAW (WING AND PYLON OUT OF PHASE)	11.260	12.595	12.629
WING TORSION	27.160	24.287	28.910

Figure 2-25

WINGTIP BOX FREQUENCY SUMMARY
PYLON AT 0° (AIRPLANE MODE)

MODE DESCRIPTION	MEASURED FREQUENCY (Hz)	ANALYSIS FREQUENCY (Hz)	
		PRETEST	POSTTEST
FIRST WING BEAMWISE BENDING	5.757	5.269	4.937
FIRST WING CHORDWISE BENDING (WING AND PYLON IN PHASE)	8.026	8.919	8.313
PYLON YAW (WING AND PYLON OUT OF PHASE)	15.078	16.385	15.057
WING TORSION	24.471	25.953	25.027

Figure 2-26

CORRELATION OF PROPROTOR STABILITY
925 RPM (104%), PYLON OFF THE DOWNSTOP

WING BEAM DAMPING, % critical

0.3% INPUT DAMPING

WING CHORD DAMPING, % critical

1.0% INPUT DAMPING

STABLE

TUNNEL AIRSPEED, KEAS

FULL SCALE AIRSPEED, KEAS

● V-22 0.2 SCALE SEMISPAN MODEL THIRD ENTRY
— ASAP ANALYSIS
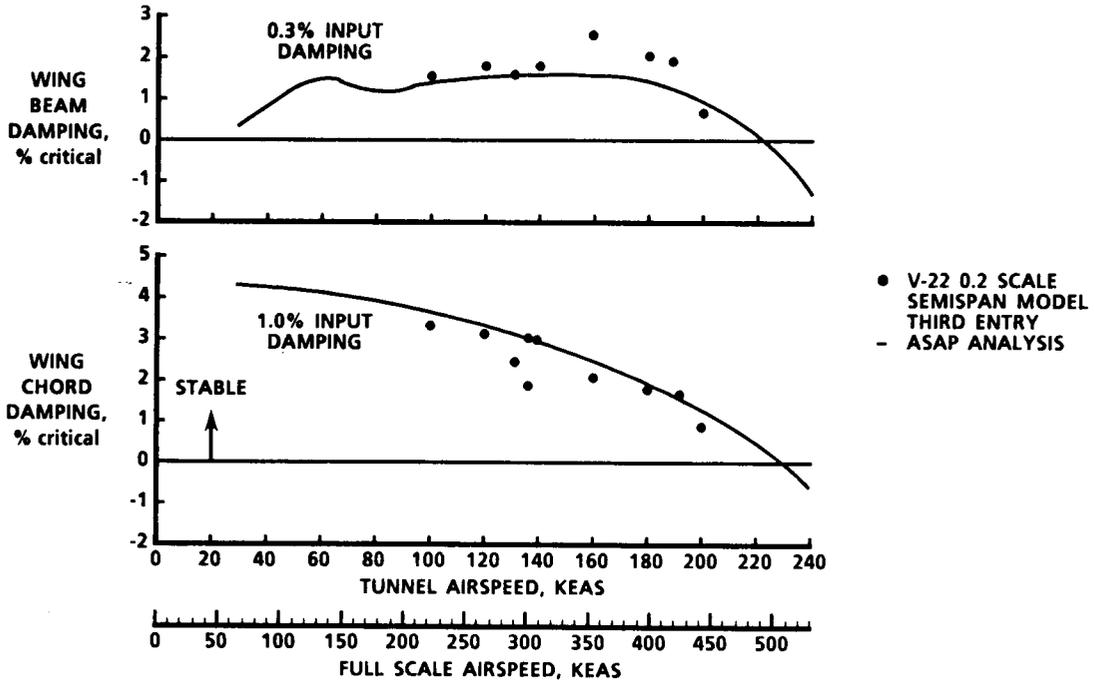
Figure 2-27

PITCH ATTITUDE RESPONSE TO LONGITUDINAL CYCLIC, 100 KIAS

GAIN, dB

C81

FLIGHT TEST

M222/688
FLIGHT 219D
GW = 7855 lb
CG = 248 in.
ALT = 1000 ft

PHASE, deg

C81 ESTIMATE MODIFIED WITH $e^{-0.145s}$ TERM

FREQUENCY, rad/sec
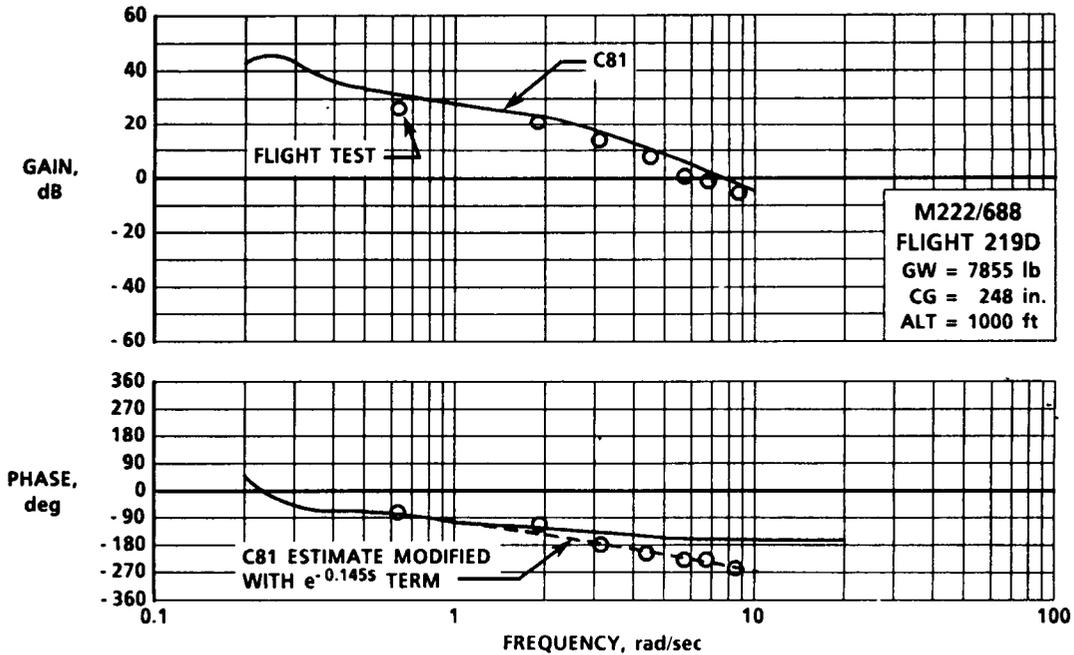
Figure 2-28

XV-15 AIRPLANE MODE, 4.2 G MANEUVER, 216 KIAS

SHIP 702   GW = 13590 lb   CG = 298.5 in.

————— FLIGHT 290, CTR 1014
— — — C81

TIME, sec   TIME, sec
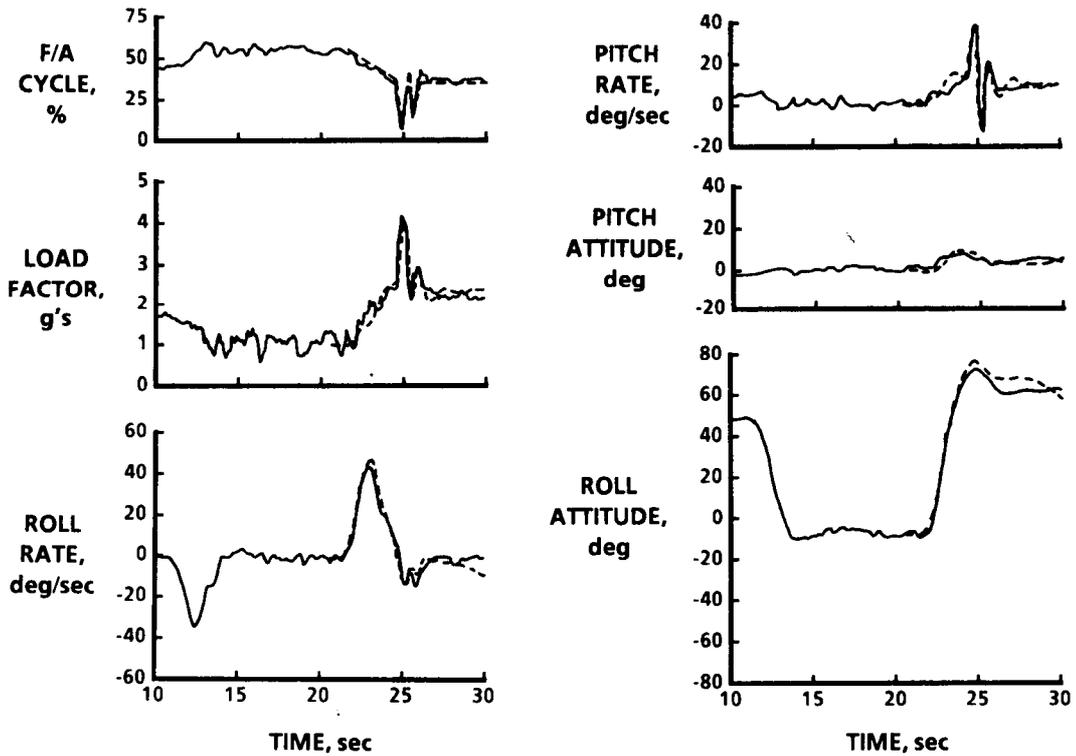
Figure 2-29

V-22 JOINT SERVICES VERTICAL LIFT TRANSPORT
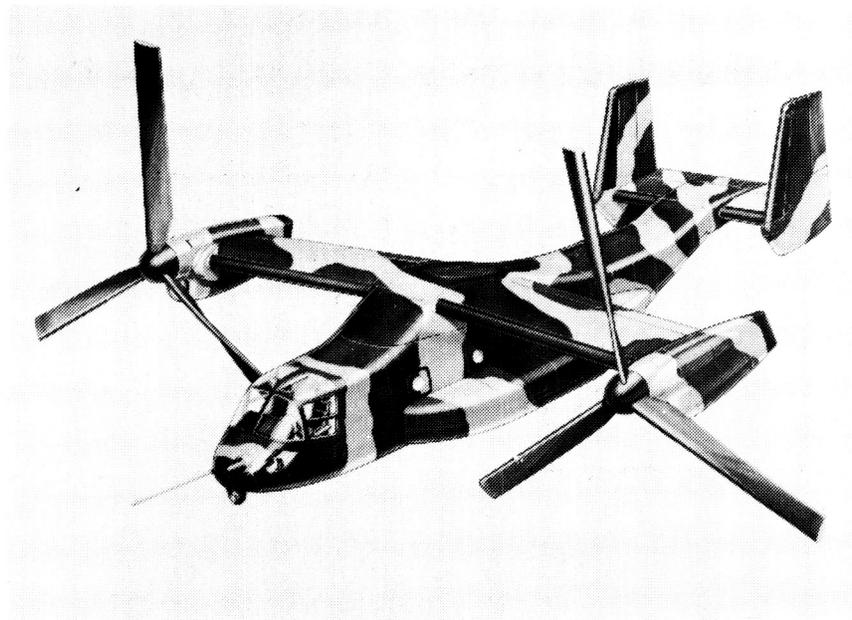
Figure 3-1

V-22 TILT ROTOR ASW AIRCRAFT

Figure 3-2

V-22 GUNSHIP

© 1987
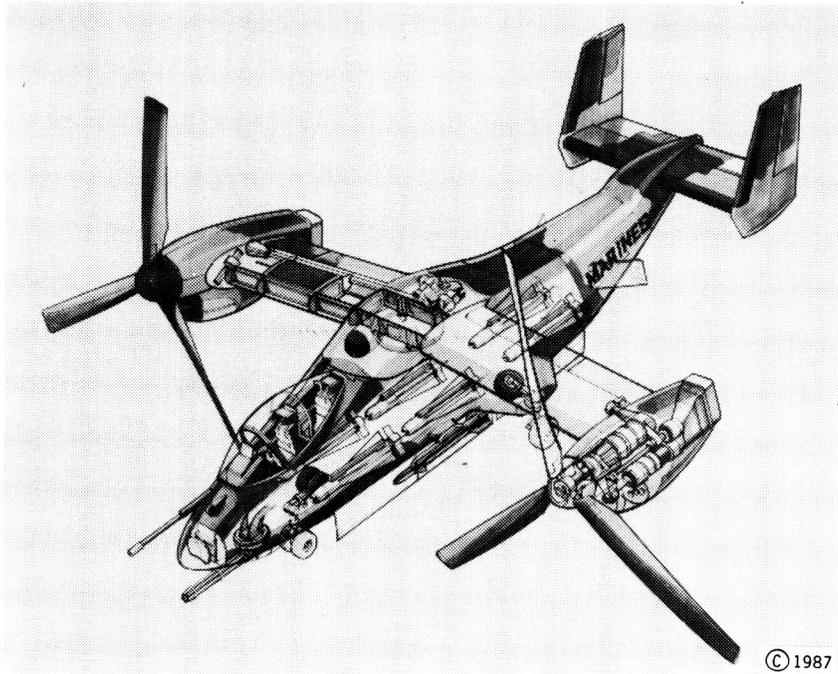
Figure 3-3

MEDIUM MIDWING GUNSHIP

© 1987
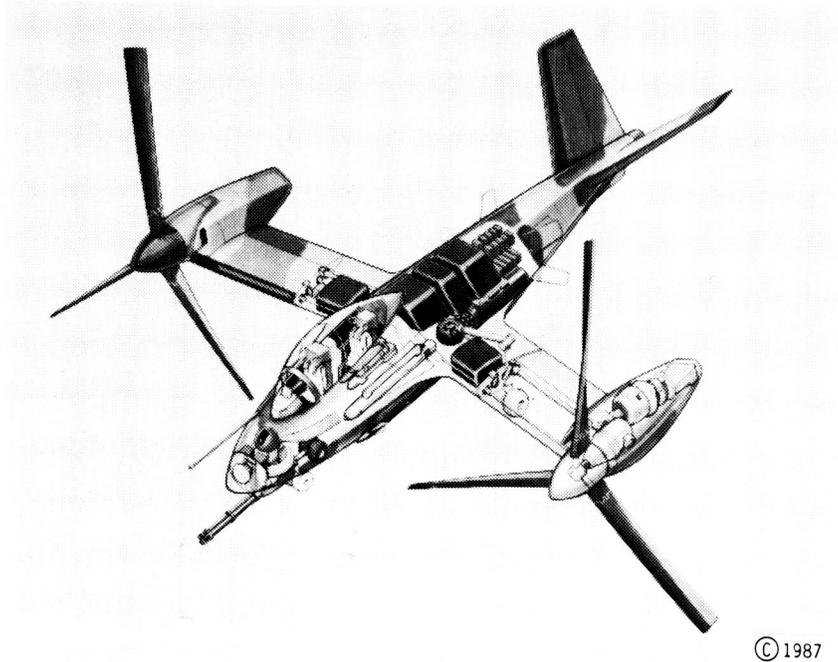
Figure 3-4

MULTIPURPOSE LIGHT TILT ROTOR GUNSHIP

©1987
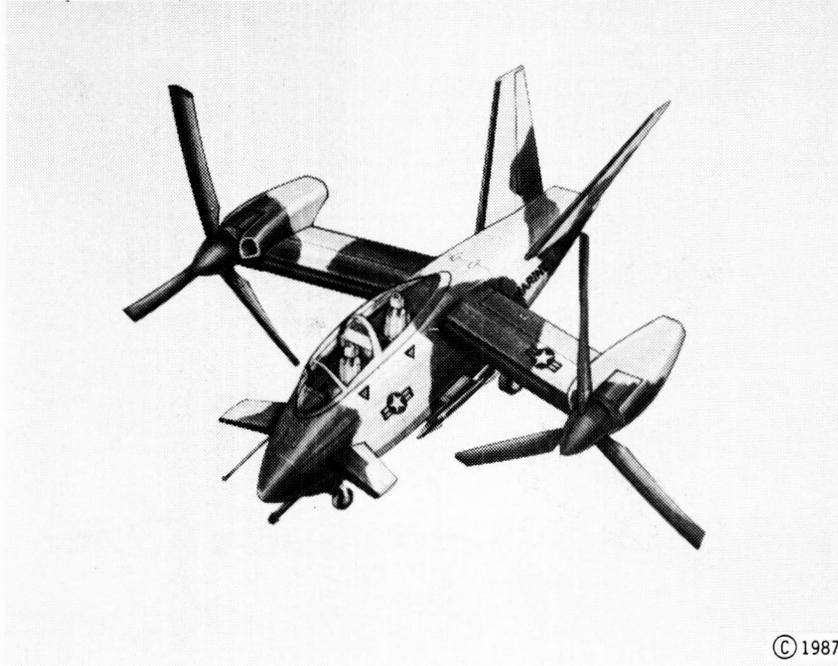
Figure 3-5

COMMERCIAL VERSION OF V-22

©1987
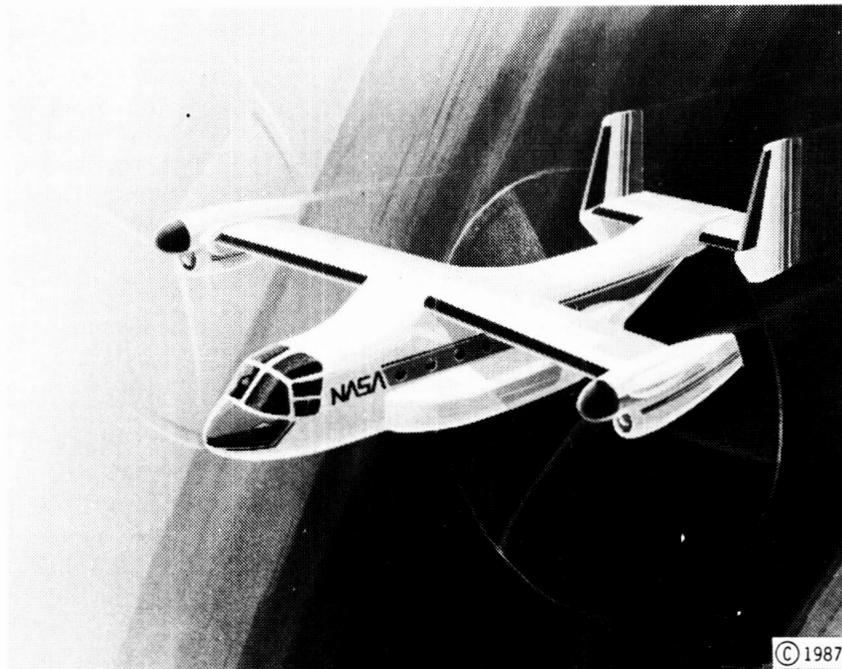
Figure 3-6

COMMERCIAL TILT ROTOR CONFIGURATION 1
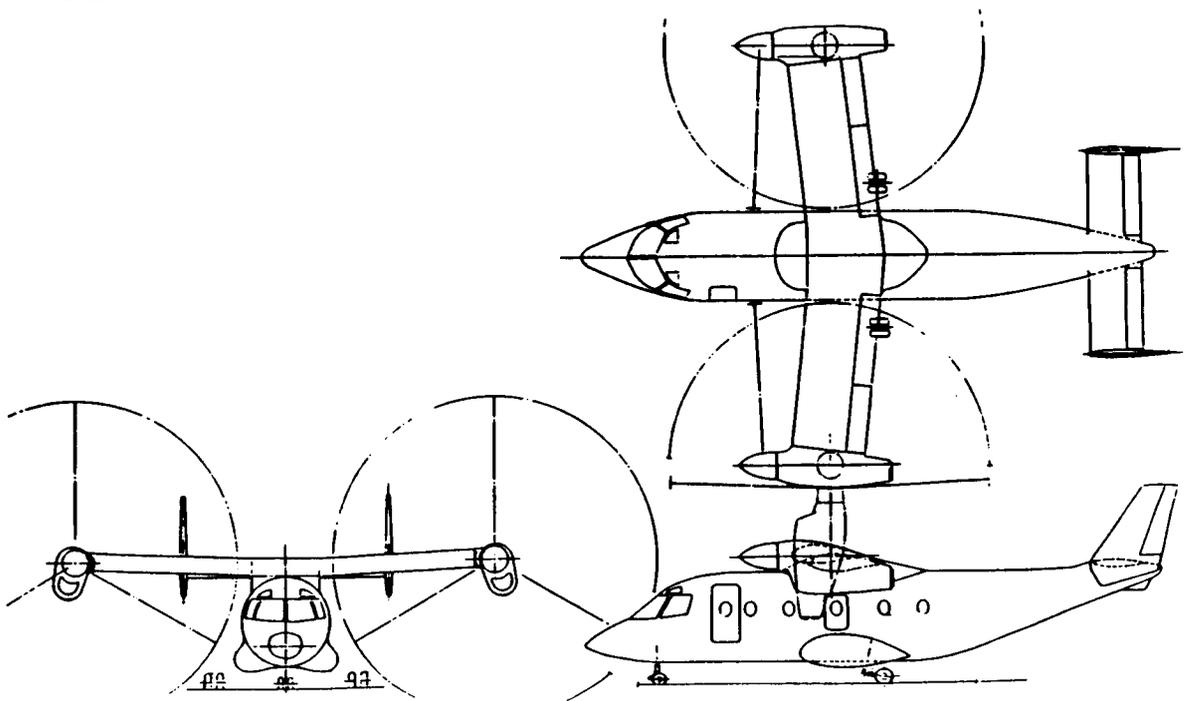
Figure 3-7

COMMERCIAL TILT ROTOR CONFIGURATION 2
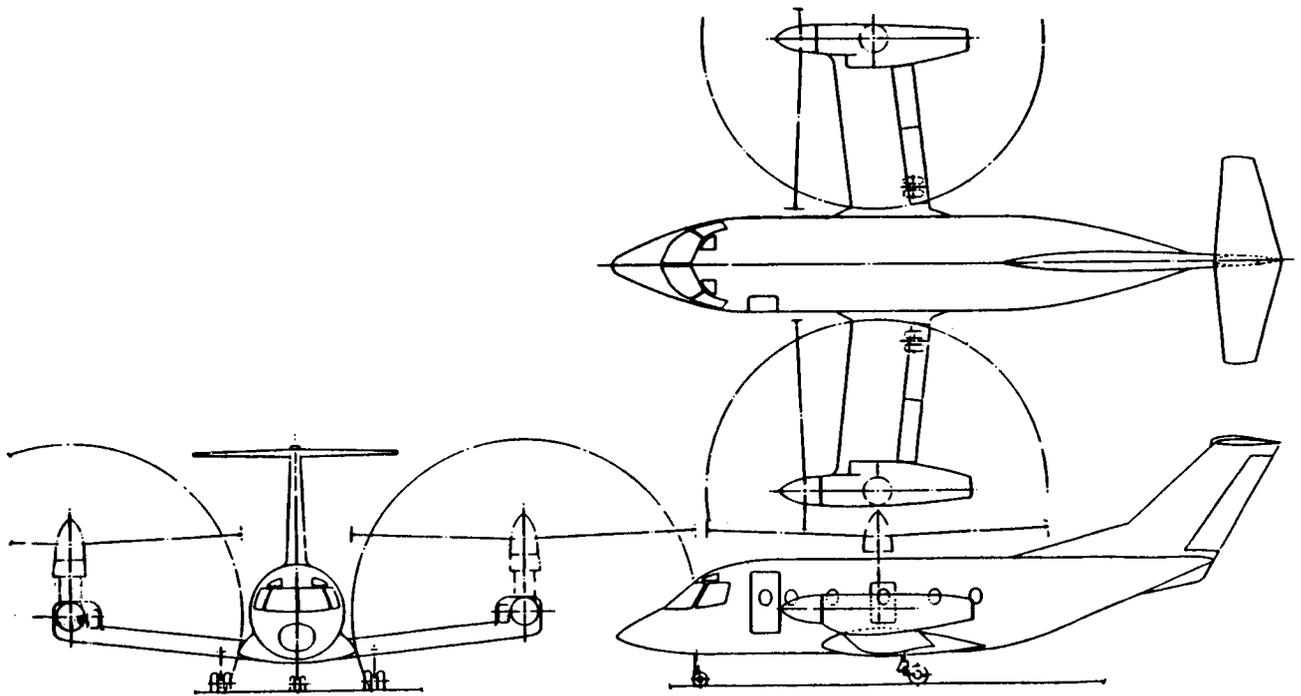
Figure 3-8

COMMERCIAL TILT ROTOR CONFIGURATION 3

① **MAX AFT CG: STA 302.0, WL 99.9**
GROSS WEIGHT: 20,125 LB

MAX GROSS WEIGHT: 22,560 LB
CG: STA 300.4, WL 100.1

② **MIN FLYING GW: 15,543 LB**
CG: STA 290.0, WL 104.6

ROTOR DIA, 28' 0"

MAXIMUM POSSIBLE REVISED

WL 171.1
WL 150.0
WL 60.0

STA 300.0

© 1987
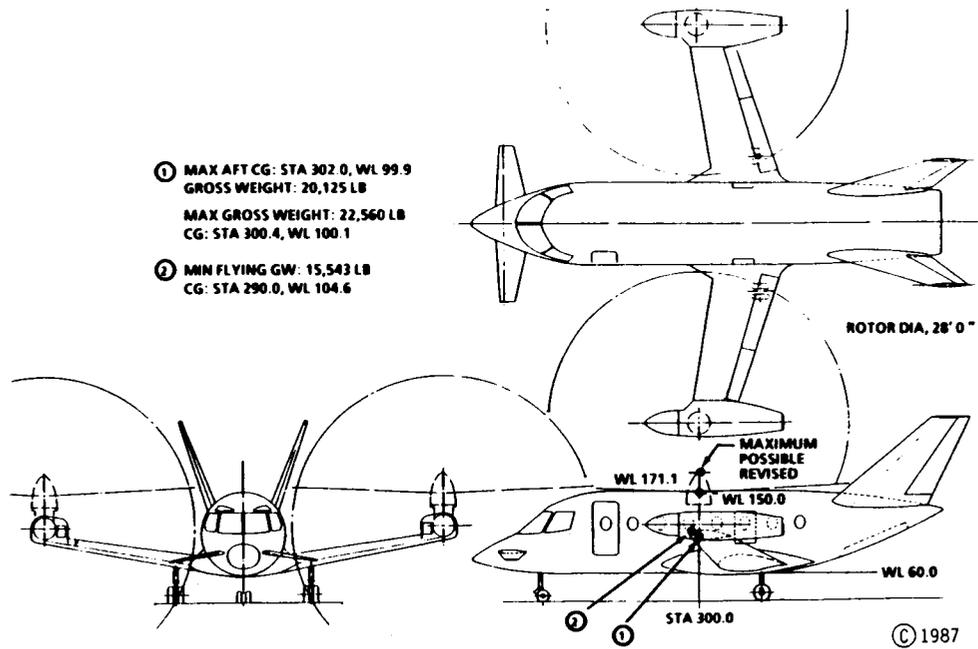
Figure 3-9

TILT ROTOR EXECUTIVE TRANSPORT

© 1987
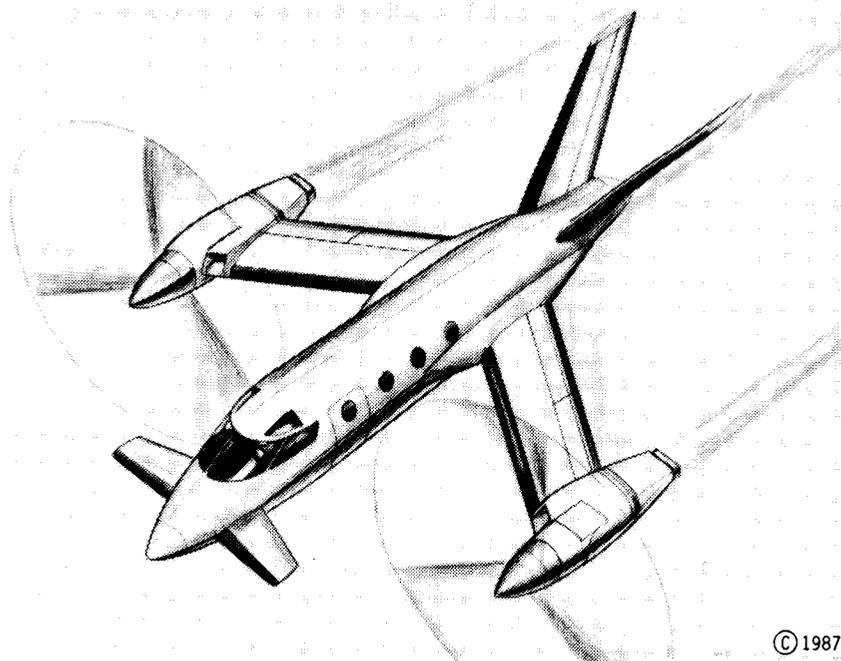
Figure 3-10

TILT ROTOR AIRLINER

©1987
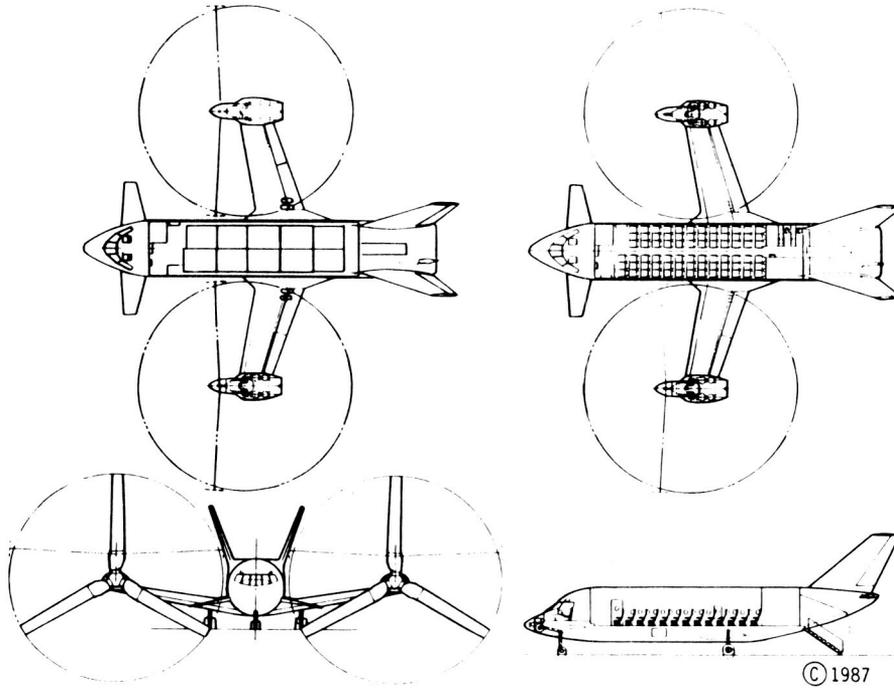
Figure 3-11

TILT-FOLD FIGHTER AIRCRAFT

©1987
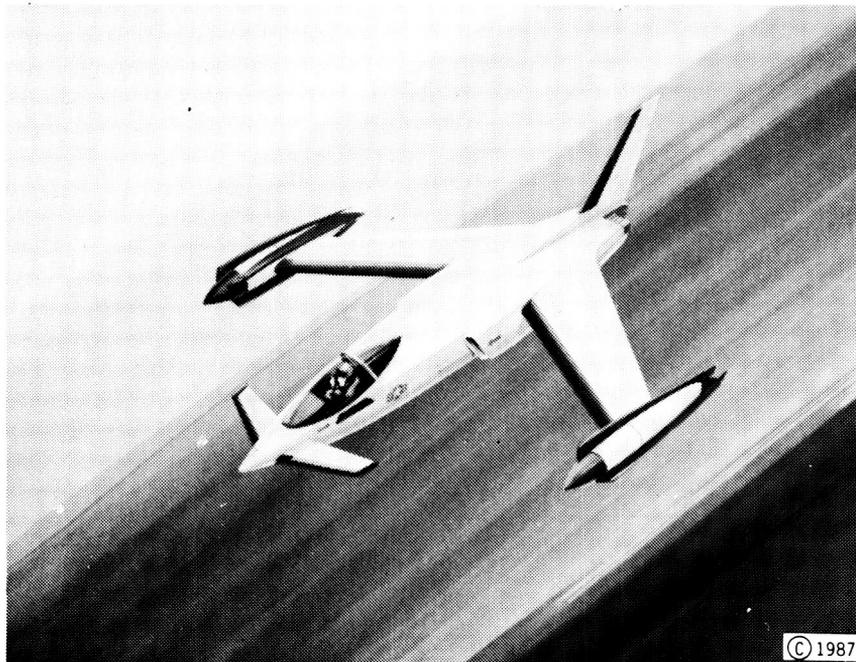
Figure 3-12

FULL-SCALE TILT-FOLD ROTOR TEST
NASA'S 40- BY 80-FOOT WIND TUNNEL
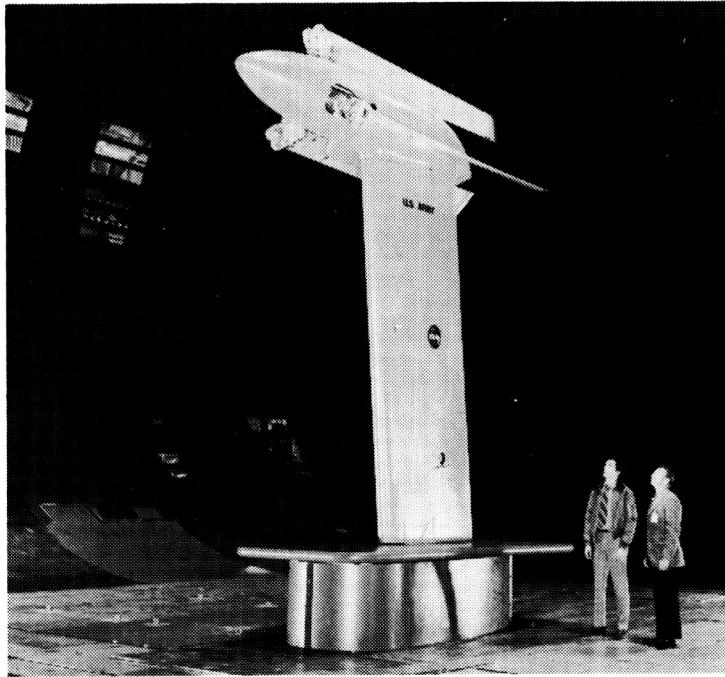
Figure 3-13

CONVERTIBLE-ENGINE CONCEPTS

CLUTCH

TO TILT FOLD
ROTORS

FAN
CLUTCH

FROM
POWER TURBINE

(a)

FIXED PITCH FAN

CLUTCH

TO TILT FOLD
ROTORS

FROM
POWER
TURBINE

(b)

VARIABLE EXHAUST
NOZZLE

VARIABLE PITCH
FAN
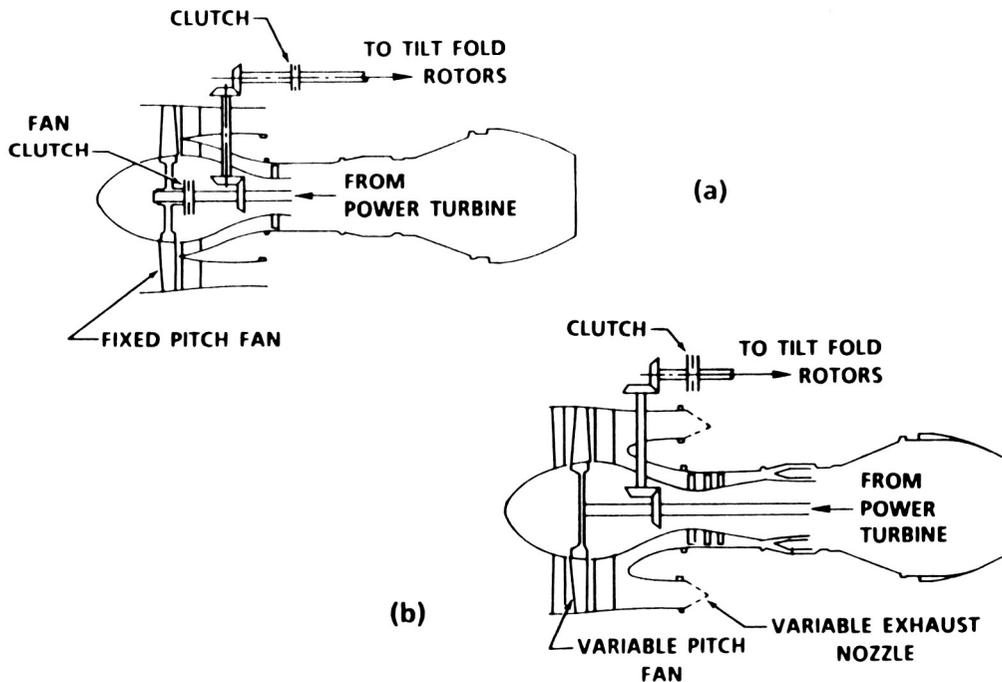
Figure 3-14

SHIPBOARD-COMPATIBLE TILT-FOLD ASW AIRCRAFT

© 1987
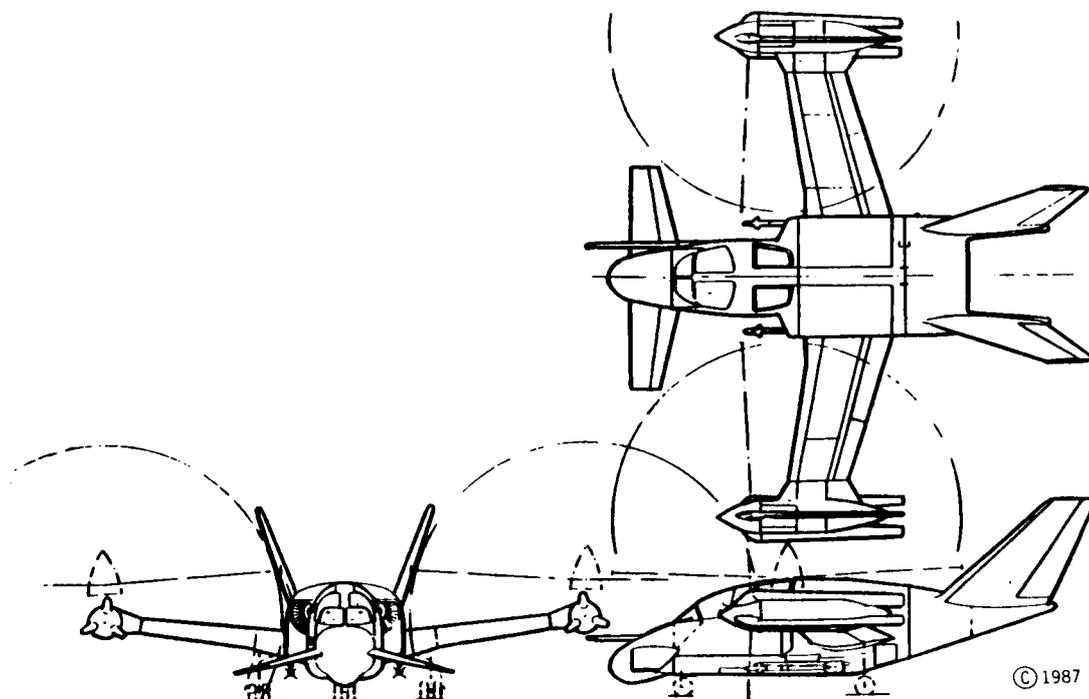
Figure 3-15

MIDRANGE RPV REQUIREMENTS

PARAMETER	REQUIREMENT
SPEED	MEDIUM TO HIGH SUBSONIC
ALTITUDE	LOW TO 30,000 FEET
MAXIMUM RANGE (RADIUS)	300 NAUTICAL MILES (EXTEND TO 400 NMI WITH AIR LAUNCH)
FLIGHT TIME	2 TO 3 HOURS
LAUNCH	GROUND, SURFACE, AIR (A-6)*

*NOT REQUIRED IF RPV HAS SUFFICIENT RANGE.

Figure 3-16

MIDRANGE RPV MISSION PROFILE

0.5 HR FOR HELICOPTER TO
LOCATE AND PICK UP RPV

2 HR OUT & BACK

1.25 HR @ 80 KN FOR
RETURN TO CARRIER

RPV CRUISE BACK

RECOVERY

RPV CRUISE OUT

A-6/RPV

RPV AIR LAUNCH

TARGET

0.5 HR
TO LAUNCH SITE

300 NMI

- TOTAL MISSION DURATION = 4.25 HR
  MISSION RADIUS = 400 NMI

RPV CRUISE BACK

CLIMB

TARGET

RPV CRUISE OUT

A-6/RPV

DESCENT

RPV LAUNCH
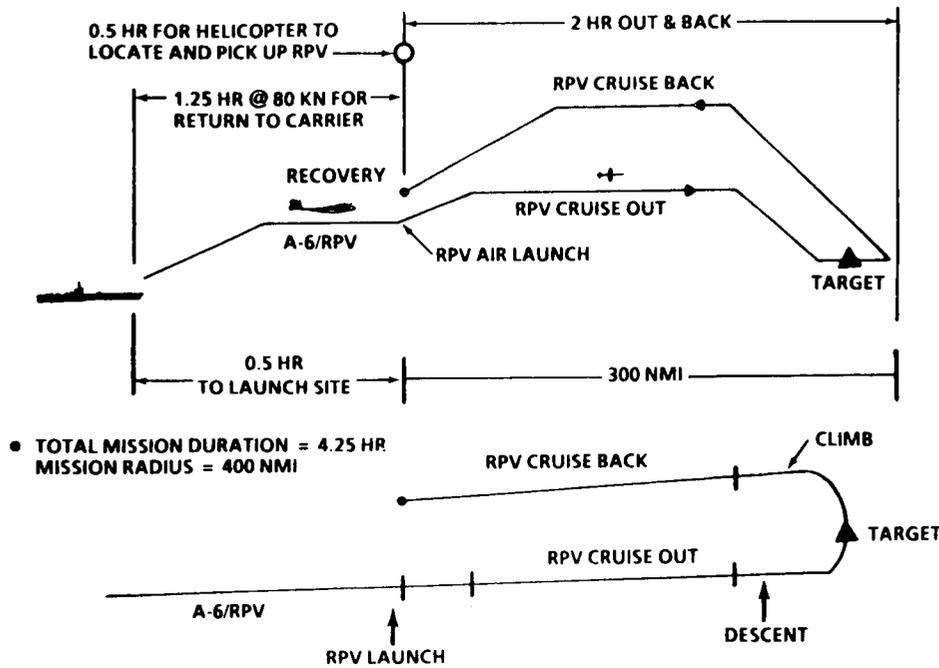
Figure 3-17

CONCEPTUAL TILT ROTOR RPV

MEDIUM RANGE
2200 POUNDS

14 FT

DIA
11.33-FT

18.5 FT

©1987

Figure 3-18

1335
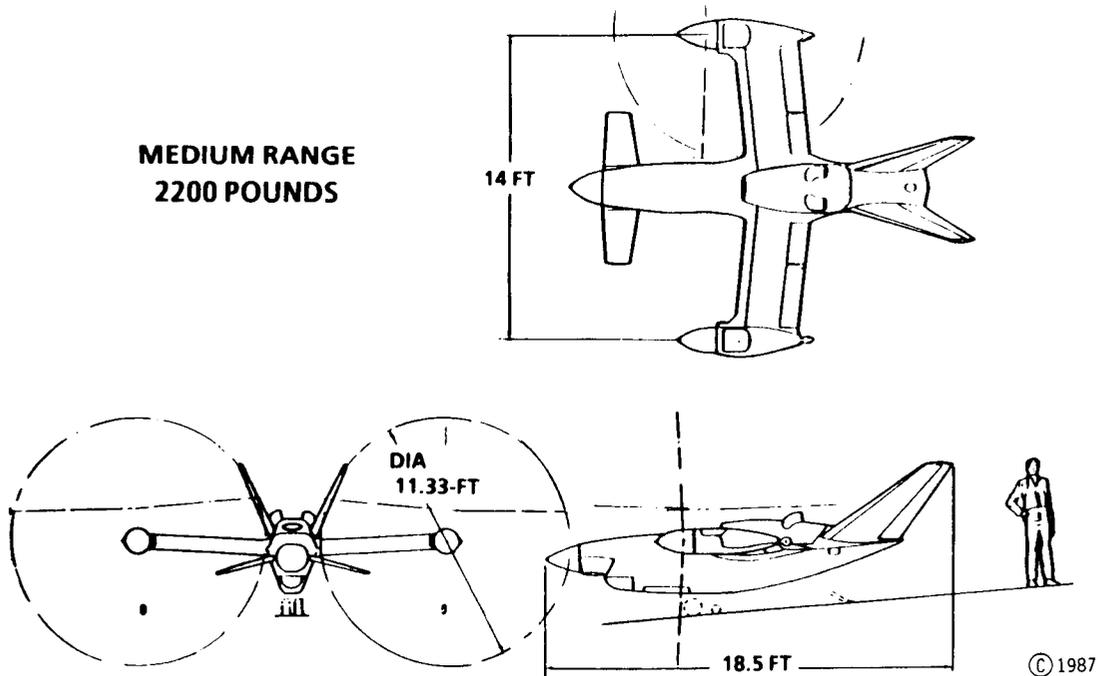
WEIGHT AND PERFORMANCE SUMMARY
2200-POUND TILT ROTOR RPV

WEIGHT

EMPTY WEIGHT	1150 LB
MAX FUEL CAPACITY	830 LB
MAX PAYLOAD ALLOWANCE	300 LB
MAX GROSS WEIGHT	2200 LB

PERFORMANCE AT 10,000 FT

MAX RANGE, 10% RESERVE	894 NMI
LONG RANGE CRUISE SPEED	204 KN
MAX SPEED	245 KN

Figure 3-19

TILT ROTOR RPV MISSION PROFILE

204-KN CRUISE SPEED @ 10,000 FT

CRUISE OUT

CRUISE BACK

NOTE: ANY VESSEL WITH A
30 X 30 FT PAD WILL DO. IT
NEED NOT BE A CARRIER!

VTOL

TARGET

|◄—————————— 400 NMI ——————————►|

- TOTAL MISSION DURATION = 4 HR
- REDUCED LIFE CYCLE COSTS
- WATER RECOVERY NOT NECESSARY
- REDUCED CAPITAL ASSETS (NO A-6, NO HELICOPTER)
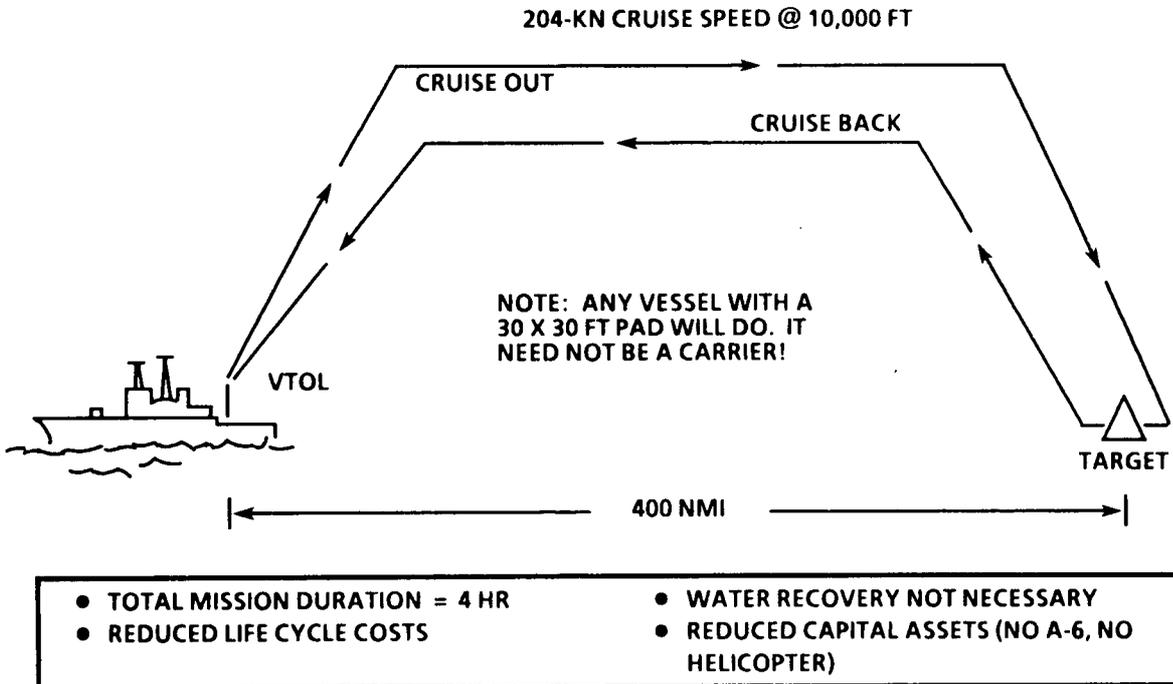
Figure 3-20

V-22 WIND TUNNEL TEST
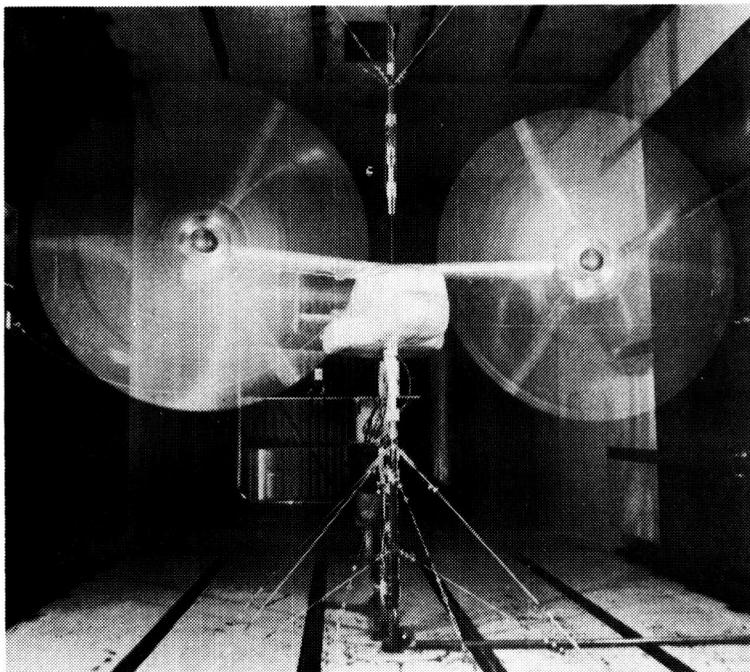
Figure 3-21

TILT ROTOR RPV DEMONSTRATOR
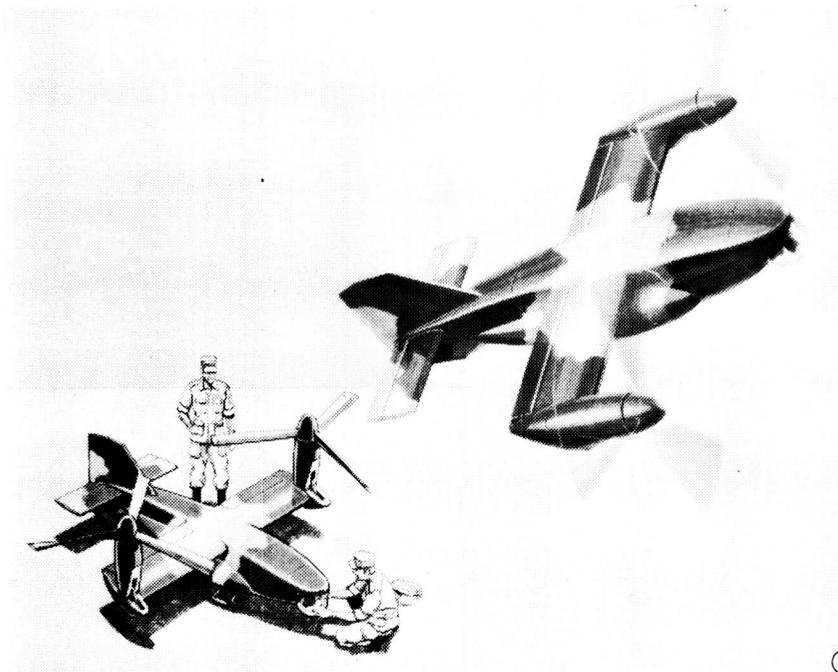
©1987

Figure 3-22

SCHEMATIC OF RPV DRIVE SYSTEM

1503 RPM

- USES OFF-THE-SHELF GEARING
- HAS ONLY 4 DIFFERENT GEAR TYPES

FWD

3007 RPM

95 HP @ 8000 RPM

6015 RPM
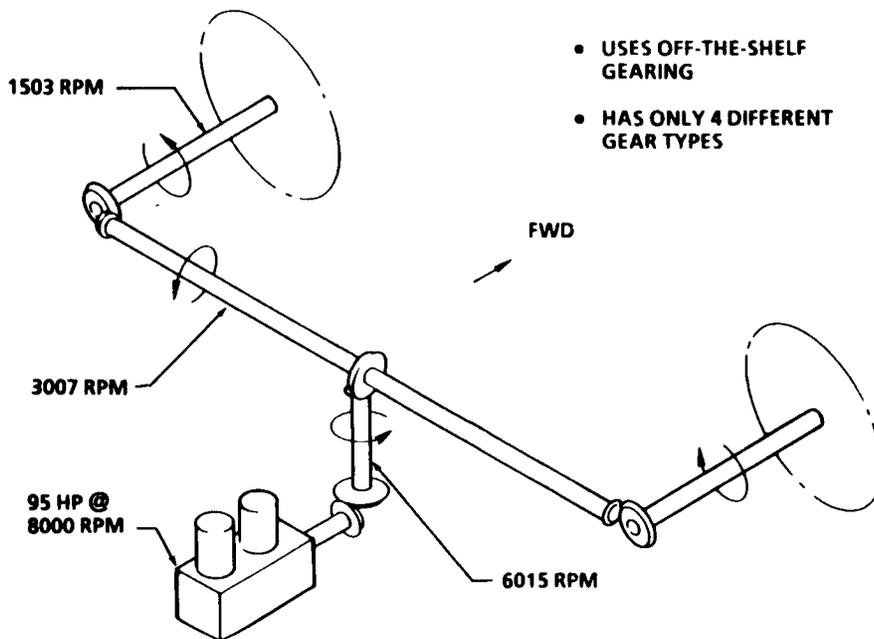
Figure 3-23

SCHEMATIC OF RPV NACELLE
CONTROL MECHANISM SIMILAR TO XV-15

COLLECTIVE ACTUATING LINK & ANTI-DRIVE

COLLECTIVE ACTUATOR

SWASHPLATE

WORM GEARBOX

DRIVE SCREW

CYCLIC ACTUATOR

UNIVERSAL JOINT

PIVOT AXIS

WING CONTOUR

DRIVE SCREW
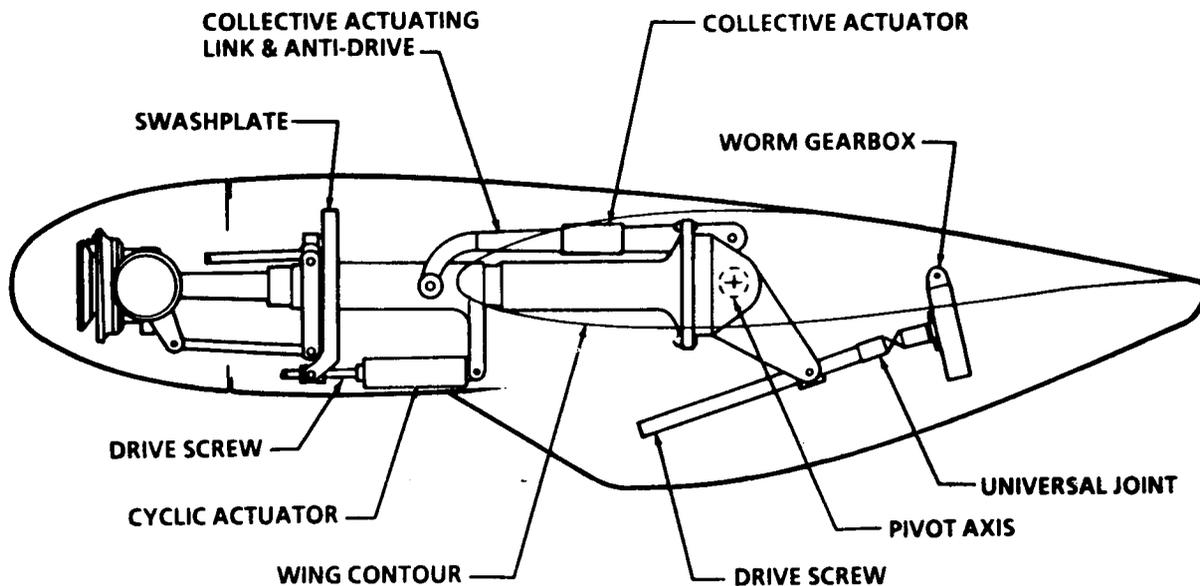
Figure 3-24

MODULAR STRUCTURE OF TILT ROTOR RPV

WING/PYLON ASSY
125 LB

BLADES (6)
2.5 LB EACH

TAIL SURFACES
16 LB

FUSELAGE
175 LB

SENSOR
75 LB

FUEL PODS (2)
5 LB EACH

TRANSPORTABLE BY 3 PEOPLE

EMPTY WT - 416 LB
FUEL   - 88
T.O. WT   504 LB
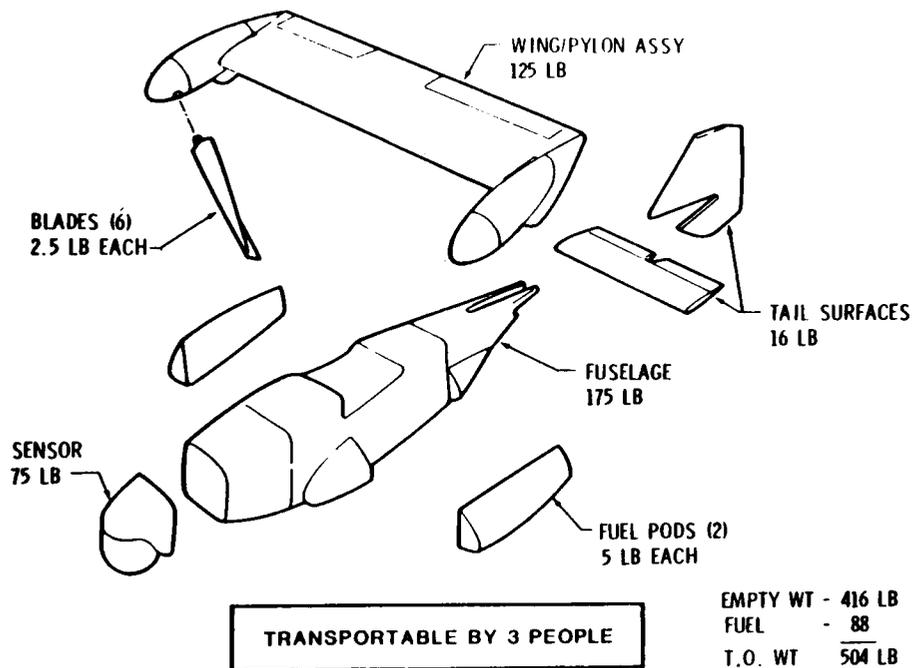
Figure 3-25

WEIGHT & PERFORMANCE SUMMARY
PRODUCTION TILT ROTOR RPV

WEIGHT

EMPTY WEIGHT	350 LB
FUEL ALLOWANCE	100 LB
PAYLOAD ALLOWANCE	75 LB

PERFORMANCE

MAX SPEED	160 KN
HOVER OGE	7,500 FT
ENDURANCE	5 + HR
CEILING	25,000 FT

Figure 3-26

SCHEDULE FOR TILT ROTOR RPV DEMONSTRATOR

Figure 3-27